PLOS | PATHOGENS

RESEARCH ARTICLE

Dual targeting of a virus movement protein to ER and plasma membrane subdomains is essential for plasmodesmata localization

Kazuya Ishikawa¤, Masayoshi Hashimoto, Akira Yusa, Hiroaki Koinuma, Yugo Kitazawa, Osamu Netsu, Yasuyuki Yamaji, Shigetou Namba*

Laboratory of Plant Pathology, Graduate School of Agricultural and Life Sciences, The University of Tokyo, 1-1-1 Yayoi, Bunkyo-ku, Tokyo, Japan

¤ Current address: Department of Botany, Graduate School of Science, Kyoto University, Kyoto, Japan
* anamba@mail.ecc.u-tokyo.ac.jp

OPEN ACCESS

Citation: Ishikawa K, Hashimoto M, Yusa A, Koinuma H, Kitazawa Y, Netsu O, et al. (2017) Dual targeting of a virus movement protein to ER and plasma membrane subdomains is essential for plasmodesmata localization. PLoS Pathog 13(6): e1006463. https://doi.org/10.1371/journal.ppat.1006463

Editor: Peter D. Nagy, University of Kentucky, UNITED STATES

Received: June 29, 2016

Accepted: June 10, 2017

Published: June 22, 2017

Data Availability Statement: All relevant data are within the paper and its Supporting Information files.

Funding: This work was supported by Grants-in-Aid for Scientific Research from the Japan Society for the Promotion of Science (KI, JSPS KAKENHI Grant Number 13J07458; SN, JSPS KAKENHI Grant Number 25221201; https://www.jsps.go.jp/english/index.html). The funders had no role in

Abstract

Plant virus movement proteins (MPs) localize to plasmodesmata (PD) to facilitate virus cell-to-cell movement. Numerous studies have suggested that MPs use a pathway either through the ER or through the plasma membrane (PM). Furthermore, recent studies reported that ER-PM contact sites and PM microdomains, which are subdomains found in the ER and PM, are involved in virus cell-to-cell movement. However, functional relationship of these subdomains in MP traffic to PD has not been described previously. We demonstrate here the intracellular trafficking of fig mosaic virus MP (MP_{FMV}) using live cell imaging, focusing on its ER-directing signal peptide (SP_{FMV}). Transiently expressed MP_{FMV} was distributed predominantly in PD and patchy microdomains of the PM. Investigation of ER translocation efficiency revealed that SP_{FMV} has quite low efficiency compared with SPs of well-characterized plant proteins, calreticulin and CLAVATA3. An MP_{FMV} mutant lacking SP_{FMV} localized exclusively to the PM microdomains, whereas SP chimeras, in which the SP of MP_{FMV} was replaced by an SP of calreticulin or CLAVATA3, localized exclusively to the nodes of the ER, which was labeled with *Arabidopsis* synaptotagmin 1, a major component of ER-PM contact sites. From these results, we speculated that the low translocation efficiency of SP_{FMV} contributes to the generation of ER-translocated and the microdomain-localized populations, both of which are necessary for PD localization. Consistent with this hypothesis, SP-deficient MP_{FMV} became localized to PD when co-expressed with an SP chimera. Here we propose a new model for the intracellular trafficking of a viral MP. A substantial portion of MP_{FMV} that fails to be translocated is transferred to the microdomains, whereas the remainder of MP_{FMV} that is successfully translocated into the ER subsequently localizes to ER-PM contact sites and plays an important role in the entry of the microdomain-localized MP_{FMV} into PD.

Author summary

Intercellular trafficking of molecules through plasmodesmata (PD) is indispensable for plant development. Plant viruses also use the intercellular trafficking system to establish

study design, data collection and analysis, decision to publish, or preparation of the manuscript.

Competing interests: The authors have declared that no competing interests exist.

systemic infection. Virus movement proteins (MPs), which have abilities to localize to PD and to move to the adjacent cells autonomously, play important roles in facilitating virus cell-to-cell movement. Hence, understanding how MPs reach PD has great significance for virology and plant cell biology. In this study, we analyzed the intracellular trafficking of fig mosaic virus movement protein (MP_{FMV}) mainly based on its N-terminal signal peptide (SP). SPs, short peptides directing proteins to the ER, are frequently found in a diverse array of proteins, but rarely found in plant virus proteins. We focused on the SP of MP_{FMV} and investigated the relationship between ER translocation and PD localization. We showed that the SP of MP_{FMV} had quite low translocation efficiency and contributes to generating two distinct populations. Each population localized to specialized subdomains of the ER and PM, and was essential for PD localization, indicating that these subdomains and PD are functionally related. Thus, our findings offer new insights into cell-to-cell movement in plants.

Introduction

Plasmodesmata (PD), channels providing symplastic continuity of the ER and the plasma membrane (PM) between adjacent cells, play vital roles in intercellular communication in plants [1]. The ER and PM passing through PD are highly specialized to regulate PD permeability [2,3]. Plant viruses must pass through PD to establish systemic infection. To modify PD function and facilitate the cell-to-cell movement, viruses have PD-targeting proteins, the so-called movement proteins (MPs) [4]. Hence, understanding how MPs reach PD will provide insight into the mechanism underlying virus cell-to-cell movement.

MPs have been frequently proposed to use a membrane trafficking pathway either through the ER or through the PM to reach PD. Several viruses possess MPs that reportedly use endomembrane trafficking through the ER. These MPs are apparently associated with the ER and PD in infected cells [5–8] or in cells transiently expressing only MPs [9], even though the detailed mechanism by which these MPs traffic from the ER to PD is unclear. On the one hand, other MPs such as those of cauliflower mosaic virus and cowpea mosaic virus localize to the PM [10,11]. Inhibition by brefeldin A (BFA), an inhibitor of COPII transport, showed that the secretory pathway is not involved in the PM localization [10,11], but how these MPs traffic to the PM is still unknown. One recent study has proposed that cauliflower mosaic virus MP is transported from the PM to PD through the endocytic pathway [12].

Recent studies have shown that two membrane subdomains in the ER and PM are also involved in virus cell-to-cell movement. ER-PM contact sites, membrane subdomains connecting between the cortical ER and the PM, are known to play roles in intracellular Ca^{2+} homeostasis and signaling in mammalian cells [13]. *Arabidopsis* synaptotagmin 1 (SYTA), a key component in connecting the cortical ER and the PM in plant cells [14,15], substantially localizes to the nodes of the cortical ER [15]. SYTA interacts with several virus MPs, and knockout or dominant-negative inhibition of SYTA delays cell-to-cell movement of several viruses [16,17]. These facts indicate that the function of ER-PM contact sites is important for virus cell-to-cell movement.

PM microdomains, small regions which have compositions and functions distinct from the surrounding PM, are another type of membrane subdomains that are involved in virus cell-to-cell movement. PM microdomains have been proposed to have lipid compositions that differ from the surrounding PM and to be detergent insoluble, although this is still a matter of debate [18]. The number and the biological roles of microdomains are largely unknown in plant cells,

but certain proteins show patchy distribution in the PM and are recognized as microdomain-associated proteins [19]. One of the microdomain-associated proteins, remorin (REM1.3), suppresses cell-to-cell movement of potato virus X (PVX) [20]. Furthermore, REM1.3 localizes also to PD and interacts with triple gene block protein 1 (TGBp1), an MP of PVX. Thus, it has been suggested that PM microdomains as well as ER-PM contact sites are important for virus cell-to-cell movement. Considering that PD localization of virus MPs is necessary for facilitating virus cell-to-cell movement, these two membrane subdomains, microdomains and ER-PM contact sites, are speculated to be involved in MP traffic to PD [16,17,20]. However, there is no direct evidence that virus MPs use these subdomains to reach PD, and a functional relationship of these subdomains in MP traffic to PD is unclear.

Signal peptides (SPs) are short sequences comprising approximately 7–30 aa that are frequently found in the N terminus of a diverse array of proteins. In general, proteins in eukaryotic cells with an SP are co-translationally recruited to the ER, and penetrate the ER membrane or are released into the ER lumen concomitant with the SP cleavage [21,22]. Some of these proteins play specific roles in the ER, whereas others are further transported to other organelles or secreted into the extracellular space. Thus, SPs are essential for proper localization and membrane targeting of proteins.

Fig mosaic virus (FMV) is a negative-strand RNA virus in the genus *Emaravirus*. We showed previously that the MP of FMV (MP_{FMV}) localized to the PM in addition to PD, and remarkably, MP_{FMV} was predicted to possess an N-terminal SP [23]. To the best of our knowledge, no viruses, other than the members of the genus *Emaravirus*, have an MP possessing an SP. In this study, we analyzed the intracellular trafficking of MP_{FMV} focusing on the SP function in hopes of determining how the recruitment of a virus MP to the ER is involved in PD targeting. As a result, we found that the SP of MP_{FMV} has extremely low ER translocation efficiency compared with conventional SPs of plant proteins, thereby causing abortive ER translocation of MP_{FMV} at a high frequency. A fraction of MP_{FMV} was translocated to the ER, whereas the remainder of MP_{FMV}, which was not translocated to the ER, was transported to the patchy microdomains in the PM. Moreover, the ER-translocated MP_{FMV} specifically localized to the ER-PM contact sites and played an essential role in the entry of microdomain-localized MP_{FMV} into PD. Taken together, these findings suggest that dual targeting to two distinct subdomains in the ER and PM is essential for PD localization of MP_{FMV}.

Results

MP_{FMV} was distributed predominantly in PD and the patchy microdomains of the PM

MP_{FMV} was fused to YFP (MP_{FMV}:YFP) to investigate its subcellular localization in *Nicotiana benthamiana*. Consistent with our previous results [23], transiently expressed MP_{FMV}:YFP localized to the punctate structures along the PM in epidermal cells (Fig 1Ai). Treatment with aniline blue, which stains callose structures including PD, showed that the punctate structures of MP_{FMV}:YFP colocalized with PD (Pearson correlation coefficient [PCC] = 0.53 ± 0.03). Measurement of the fluorescent intensity across plasmodesma shows that the fluorescence signal of MP_{FMV}:YFP coincided with that of aniline blue (Fig 1Aii), showing that MP_{FMV}:YFP localized to PD.

MP_{FMV}:YFP appeared to accumulate also on the PM. PM and PD localization can be easily distinguished in plasmolyzed cells because PM proteins are associated with Hechtian strands, which are stretched PMs connecting the retracted PM and the cell wall, whereas PD proteins are retained in PD even during plasmolysis [24]. In plasmolyzed cells, MP_{FMV}:YFP fluorescence was observed in Hechtian strands and PD (Fig 1Bi). On the other hand, fluorescence

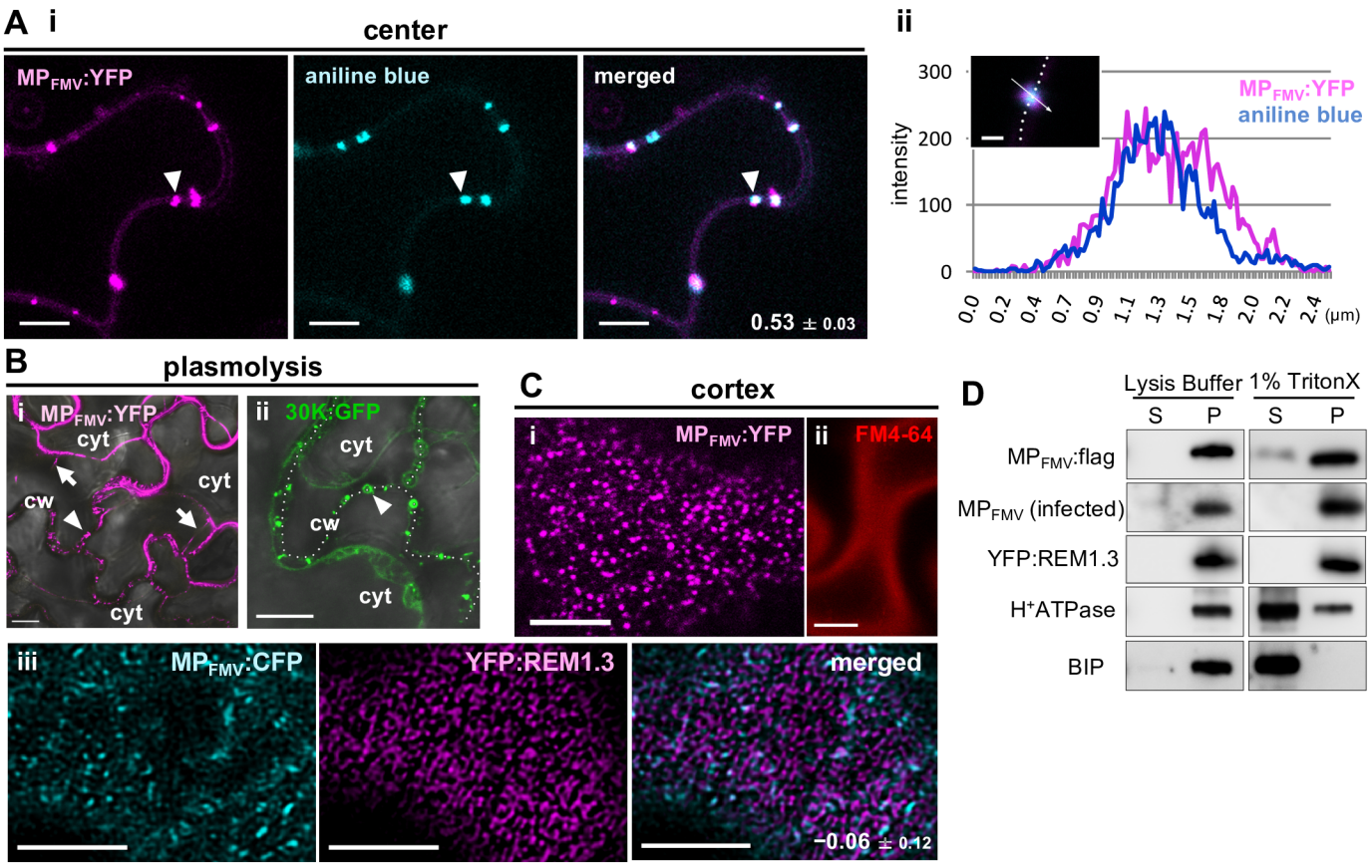

Fig 1. Investigation of the subcellular distribution of MP$_{FMV}$:YFP. (A–C) Confocal imaging of MP$_{FMV}$:YFP-expressing epidermal cells at 36 hours post-infiltration (hpi). YFP fluorescence was pseudocolored by magenta. (A) (i) Cells expressing MP$_{FMV}$:YFP were treated with aniline blue. Arrowheads indicate plasmodesma. The mean ± SD of Pearson correlation coefficient (PCC [−1:1]) is given in the image. Bars = 5 μm. (ii) Fluorescence intensity along the arrow across plasmodesma. The dotted line in the confocal image indicates the cell wall. Bar = 1 μm. (B) Plasmolyzed cells expressing (i) MP$_{FMV}$:YFP or (ii) 30K:GFP. Arrows indicate Hechtian strands extended from the PM. Arrowheads indicate plasmodesmata. The dotted line indicates the cell wall. cw, cell wall; cyt, cytoplasm. Bars = 10 μm. (C) Surface views of cells (i) expressing MP$_{FMV}$:YFP or (ii) treated with FM4-64. (iii) Co-expression of MP$_{FMV}$:CFP and YFP:REM1.3. To obtain higher resolution images, images were processed by a deconvolution algorithm. Bars = 5 μm. (D) 1% TritonX-100 treatment of membranes. Membrane-enriched fractions prepared from FMV-infected fig leaves and *N. benthamiana* leaves expressing MP$_{FMV}$:FLAG or YFP:REM1.3 at 36 hpi were treated with 1% TritonX-100. Anti-FLAG, anti-MP$_{FMV}$, anti-GFP, anti-H$^+$ATPase and anti-BIP antibodies were used for the detection of MP$_{FMV}$:FLAG, MP$_{FMV}$, YFP:REM1.3, a PM marker H$^+$ATPase and an ER marker BIP. S; soluble fraction. P; insoluble fraction.

https://doi.org/10.1371/journal.ppat.1006463.g001

signal was observed only in PD, but not in Hechtian strands, when cells expressing tobacco mosaic virus MP as a GFP fusion (30K:GFP) were plasmolyzed (Fig 1Bii). These results indicate that MP$_{FMV}$:YFP accumulated in the PM, in addition to PD. Observation of the cell surface revealed that MP$_{FMV}$:YFP shows patchy distribution throughout the PM (Fig 1Ci). This distribution pattern was different from the fluorescence pattern of the PM stained with FM4-64, an amphiphilic styryl dye which is inserted into the outer layer of the PM (Fig 1Cii). These images were taken in the abaxial surface of the abaxial epidermal cells, and PD were not contained in these patches. Since such uneven distribution in the PM is similar to the localization of microdomain-associated proteins remorines [19,20], a YFP fusion with *A. thaliana* REM1.3 (YFP:REM1.3) was co-expressed with MP$_{FMV}$:CFP; however, YFP:REM1.3 did not substantially co-localize with MP$_{FMV}$:CFP (PCC = −0.06 ± 0.12; Fig 1Ciii). MP$_{FMV}$ probably localized to the PM subdomains distinct from those of REM1.3.

To corroborate the subcellular distribution of MP_{FMV} observed by microscopy, we performed chemical treatment using 1% TritonX-100. 1% TritonX-100 was expected to solubilize proteins associated with the cellular membranes excluding proteins localized to detergent-insoluble domains, including PM microdomains [25]. As expected, TritonX-100 treatment solubilized the majority of a PM marker H^+ATPase and an ER marker BIP (Fig 1D). Conversely, only a small proportion of transiently expressed MP_{FMV}:FLAG was soluble in 1% TritonX-100. In FMV-infected cells, almost all MP_{FMV} was detected from insoluble fraction. MP_{FMV} became more insoluble in FMV-infected cells probably due to other virus factors. Furthermore, this result was in agreement with that of YFP:REM1.3, which localizes to the Triton-insoluble microdomains [19,20]. Given that MP_{FMV} unevenly distributed in the PM and that did not colocalize with REM1.3 (Fig 1Ciii), MP_{FMV} may localize to the detergent-insoluble microdomains different from those of REM1.3.

MP_{FMV} has an ER-directing signal peptide at the N-terminus

An ER-directed SP was predicted at the N-terminus of MP_{FMV} by SignalP software in our previous work [23]. The cleavage site was between G19 and M20, and the length of the deduced SP was 19 aa (Fig 2A). To verify the cleavage at the predicted site, MP_{FMV}:FLAG expressed transiently in *N. benthamiana* was purified by immunoprecipitation using anti-FLAG antibody. Immunoblot analysis using anti-FLAG antibody and Coomassie Brilliant Blue (CBB) staining of the immunoprecipitated samples showed a protein band of approximately 37 kD, indicating that precipitated MP_{FMV}:FLAG has a single molecular weight (Fig 2B). Amino acid sequences beginning at M20, but not at the N-terminal methionine, were found in the sequences determined by Edman degradation of the purified MP_{FMV}:FLAG, which means that the N-terminal 19 aa was cleaved off (S1 Fig). Combined with CBB staining and immunoblot analysis, the N-terminal 19 aa was suggested to be almost perfectly processed from MP_{FMV}:FLAG. The N-terminal 19 aa had characteristics of SPs, a central hydrophobic region which forms an α-helix and a polar C-terminal region (Fig 2C) [21,22]. These results suggest that

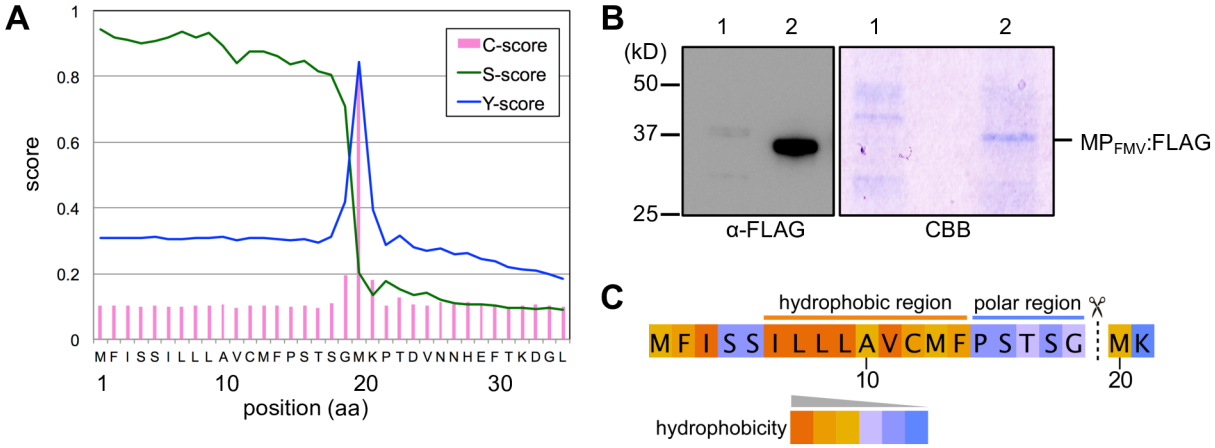

Fig 2. MP_{FMV} has an N-terminal signal peptide. (A) SignalP ver 4.1 predicted an N-terminal signal peptide in the MP_{FMV} sequence. C-score is the predicted cleavage site value, S-score is the predicted signal peptide value and Y-score is the cleavage site value calculated by combining C- and S-scores. (B) Immunoprecipitation of MP_{FMV}:FLAG. MP_{FMV}:FLAG was immunoprecipitated with anti-FLAG antibody from cell lysates of healthy control leaves (lane 1) or of MP_{FMV}:FLAG expressing leaves at 48 hpi (lane 2). The immunoprecipitated samples were checked by immunoblot analysis using anti-FLAG antibody (left panel) and Coomassie Brilliant Blue (CBB) staining (right panel). The lane between lane 1 and 2 is blank in CBB staining. (C) Hydrophobicity of the predicted SP sequence. Amino acid residues are color-coded according to their hydrophobicity. The dotted line with scissors indicates the putative cleavage site.

https://doi.org/10.1371/journal.ppat.1006463.g002

MP_{FMV} has an N-terminal SP (hereafter referred to as SP_{FMV}), which is expected to translocate the nascent protein into the ER.

SP_{FMV} has extremely low translocation efficiency

To confirm whether or not SP_{FMV} translocates a protein into the ER lumen as those of plant proteins, we constructed GFPs flanked with the N-terminal SPs derived from MP_{FMV} or plant proteins (sporamin A, calreticulin or CLAVATA3) and a C-terminal ER retention signal (Fig 3A; SP_{FMV}GFP:HDEL, SP_{spo}GFP:HDEL, SP_{cal}GFP:HDEL and SP_{clv}GFP:HDEL, respectively). We selected these three SPs because the SP activity was empirically assessed in previous studies [26–28]. These four SPs including SP_{FMV} have no sequence homology (S2 Fig). As controls, we prepared free GFP and GFP:HDEL. Here, it is noted that GFP:HDEL does not have an N-terminal SP. Unexpectedly, transiently expressed SP_{FMV}GFP:HDEL was distributed throughout the cytosol, but not to the ER (Fig 3B). The fluorescence pattern appeared to be the same as that of free GFP or GFP:HDEL. In contrast, SP_{spo}GFP:HDEL, SP_{cal}GFP:HDEL and SP_{clv}GFP:HDEL predominantly localized in the ER, as expected. These results indicate the functional difference in ER translocation between SP_{FMV} and the other SPs.

We further investigated the ER translocation ability of these SPs using N-glycosylation as an indicator. We constructed fusion proteins in which the 3× N-glycosylation sequon was C-terminally fused to GFP, SP_{FMV}GFP, SP_{spo}GFP, SP_{cal}GFP and SP_{clv}GFP (Fig 3C; GFPglc, SP_{FMV}GFPglc, SP_{spo}GFPglc, SP_{cal}GFPglc and SP_{clv}GFPglc, respectively) [29]. If an SP successfully translocates the GFP fusion into the ER lumen after SP cleavage by an ER membrane-bound SP peptidase on the lumenal side, glycosylation of asparagine residues in the sequon by an ER-resident enzyme, oligosaccharyl transferase, occurs and results in an increase in the molecular weight of the translocated GFPglc relative to that of the non-translocated GFPglc. Immunoblot analysis of total proteins extracted from leaves expressing GFPglc, SP_{FMV}GFPglc, SP_{spo}GFPglc, SP_{cal}GFPglc or SP_{clv}GFPglc using anti-GFP antibody showed that almost all of the SP_{cal}GFPglc or SP_{clv}GFPglc molecules were glycosylated (91.9% and 93.0%, respectively), and that more than half (70.9%) of the SP_{spo}GFPglc molecules were glycosylated (Fig 3D and 3E). However, compared with these measurements, a dramatically lower proportion (4.3%) of the SP_{FMV}GFPglc molecules were glycosylated. No glycosylation was detected in GFPglc, which lacks an SP. Thus, SP_{FMV} had much lower translocation efficiency compared with conventional SPs, suggesting that only a small proportion of MP_{FMV} molecules were translocated to the ER. In the case of SP_{FMV}GFP:HDEL (Fig 3B), the fluorescence of ER-translocated GFP was thought to be masked by GFP fluorescence in the cytosol because SP_{FMV} translocated only a small fraction of GFP molecules into the ER.

The subcellular localization pattern of MP_{FMV} is altered depending on the SP

To gain insight into the role of ER translocation in the intracellular trafficking of MP_{FMV}, we constructed an MP_{FMV} mutant whose SP was not expected to be cleaved (ncMP). In this mutant, two substitutions, L7P and V11P, were introduced into the central α-helix region of SP_{FMV} to break the helix [21]. We verified that an SP was no longer predicted in the ncMP sequence by SignalP (S3A Fig). Transiently expressed ncMP as a YFP fusion ($ncMP_{FMV}$:YFP) showed aberrant accumulation in the cytoplasm (S3Bi Fig), and did not target to the ER, PM and PD (S3Bii Fig). This result indicates that the cleavage of SP_{FMV} is essential for MP_{FMV} to localize properly.

We assessed localization of an MP_{FMV} mutant lacking the N-terminal 19 aa SP. The SP-deficient mutant was fused with YFP (Trun:YFP) and expressed in the same conditions as

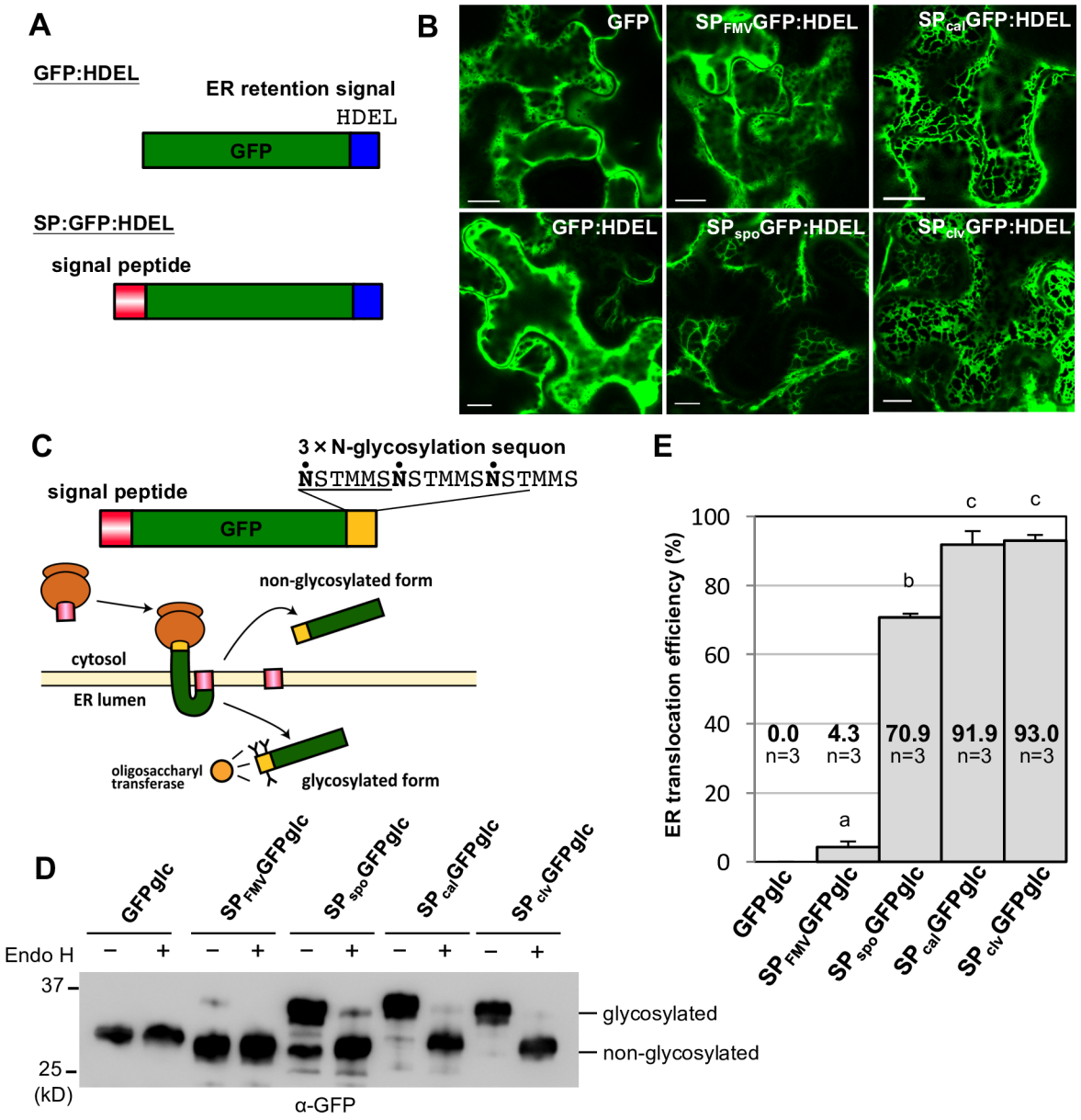

Fig 3. ER translocation efficiency of SP_{FMV} differs from those of plant protein SPs. (A) Schematic representation of fusion proteins for investigating ER translocation efficiency. (B) Cells expressing free GFP, GFP:HDEL, SP_{FMV}GFP:HDEL, SP_{spo}GFP:HDEL, SP_{cal}GFP:HDEL and SP_{clv}GFP:HDEL were observed at 36 hpi. Bars = 10 μm. (C) Schematic representation of the experimental system and fusion proteins with a 3×N-glycosylation sequon. Dots indicate asparagine residues expected to be glycosylated. SPs of MP_{FMV}, sporamin A, calreticulin or CLAVATA3 were fused to the N terminus of GFP:glc, GFP carrying a 3×N-glycosylation sequon in its C terminus (SP_{FMV}GFPglc, SP_{spo}GFPglc, SP_{cal}GFPglc and SP_{clv}GFPglc, respectively). (D) Immunoblot analysis of proteins extracted from cells expressing GFPglc, SP_{FMV}GFPglc, SP_{spo}GFPglc, SP_{cal}GFPglc or SP_{clv}GFPglc using anti-GFP antibody. Samples were collected at 30 hpi. Glycosylation of each sample was confirmed by deglycosylation with Endo H. (E) Quantitation of translocation efficiencies. The bars show means + SD of three independent experiments. Different letters on the error bars indicate statistical differences at the 1% level of significance (Tukey test).

https://doi.org/10.1371/journal.ppat.1006463.g003

MP_{FMV}:YFP in Fig 1. Trun:YFP was distributed to the PM microdomains, similar to MP_{FMV}:YFP (Fig 4Ai, compared with Fig 1Ci). The PM localization of Trun:YFP was checked by the fluorescence in Hechtian strands of plasmolyzed cells as was the case for MP_{FMV}:YFP (Fig 4Av left panel). Co-expression with ER-CFP showed that Trun:YFP was not associated with the

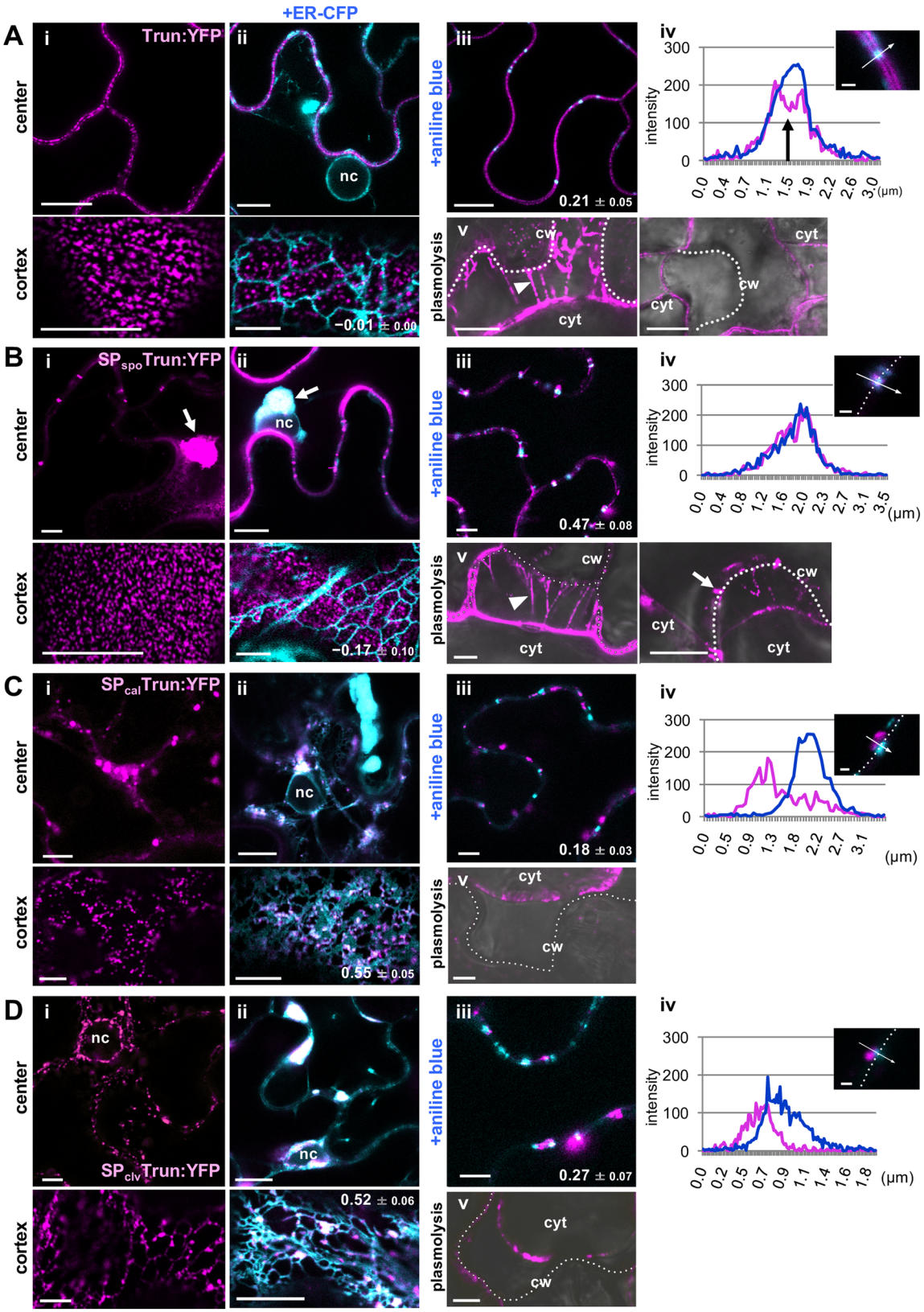

Fig 4. Deletion or replacement of SP_{FMV} alters the subcellular distribution of MP_{FMV}. Localization analysis of (A) SP-deficient MP_{FMV}, Trun:YFP, and SP chimeras; (B) SP_{spo}Trun:YFP, (C) SP_{cal}Trun:YFP and (D) SP_{clv}Trun:YFP. Images

through the center or through the cortex of cells expressing (i) Trun:YFP, SP_{spo}Trun:YFP, SP_{cal}Trun:YFP and SP_{clv}Trun:YFP alone or (ii) with ER-CFP. Arrows indicate aggregations of SP_{spo}Trun:YFP in the ER. nc; nucleus. (iii) Aniline blue treatment. (iv) Fluorescence intensity along the arrows across PD. A black arrow indicates the signal reduction of Trun:YFP in the center of PD. Dotted lines in the confocal image indicate the cell wall. Bar = 1 μm. (v) Plasmolysis. Bright-field images were merged. The dotted lines indicate the cell wall. Arrowheads indicate Hechtian strands extended from the PM (The left panels in A and B). The white arrow indicates fluorescence signals retained in PD (The right panels in B). cw, cell wall; cyt, cytoplasm. All images were captured at 36 hpi. YFP fluorescence is pseudocolored with magenta. Bars: (i)–(iii) and (v), 10 μm; (iv), 1 μm.

https://doi.org/10.1371/journal.ppat.1006463.g004

perinuclear or peripheral ER (PCC = −0.01 ± 0.00; Fig 4Aii). Also, Trun:YFP did not specifically localize to aniline blue-stained PD (PCC = 0.21 ± 0.05; Fig 4Aiii). The fluorescent signal of Trun:YFP was reduced in the region corresponding to the center of PD (Fig 4Aiv), unlike MP_{FMV}:YFP (Fig 1Aii). Furthermore, we confirmed that Trun:YFP was not retained in PD in plasmolyzed cells (Fig 4Av right panel). These results indicate that the SP-deficient mutant did not localize to PD and that the SP_{FMV} is essential for the PD localization of MP_{FMV}, but dispensable for targeting the PM microdomains.

Next, SP_{FMV} function was compared with SPs derived from plant proteins, sporamin A, calreticulin or CLAVATA3, by analyzing localization of SP chimeras in which the SPs of these proteins were fused to the N-terminus of Trun:YFP (SP_{spo}Trun:YFP, SP_{cal}Trun:YFP and SP_{clv}Trun:YFP, respectively). SP_{spo}Trun:YFP localized to the PM microdomains (Fig 4Bi, 4Bii and 4Bv) and PD (PCC = 0.47 ± 0.08; Fig 4Biii and 4Biv), similar to MP_{FMV}:YFP. However, unlike MP_{FMV}:YFP, cytoplasmic aggregations were observed in the SP_{spo}Trun:YFP-expressing cells (Fig 4Bi). Co-expression with the ER marker ER-CFP showed that these aggregations were formed in the ER (Fig 4Bii). On the other hand, SP_{cal}Trun:YFP and SP_{clv}Trun:YFP were associated with nodes in the ER network (PCC: 0.55 ± 0.05 and 0.52 ± 0.06, respectively; Fig 4Ci, Cii, 4Di and 4Dii). Although some of these punctate spots were located in close proximity to PD, many of them did not co-localize with PD (PCC: 0.18 ± 0.03 and 0.27 ± 0.07, respectively; Fig 4Ciii and 4Diii). Fluorescence intensity measurements confirmed that fluorescence signals of SP_{cal}Trun:YFP and SP_{clv}Trun:YFP did not coincide with that of aniline blue (Fig 4Civ and 4Div). Hechtian strands were invisible when cells expressing SP_{cal}Trun:YFP or SP_{clv}Trun:YFP were plasmolyzed (Fig 4Cv and 4Dv), indicating that these chimeras were not distributed to the PM. These observations suggest that SP_{FMV} plays an essential role in MP_{FMV} localization.

PD localization is necessary for exerting MP_{FMV} functions

Our previous study showed that the expression of MP_{FMV} complements cell-to-cell movement of movement-deficient PVX mutant (PVXΔTGBp1-GFP) [23]. We investigated whether MP_{FMV} mutants (Trun, SP_{spo}Trun and SP_{cal}Trun) facilitate virus cell-to-cell movement using this system. SP_{clv}Trun was not used in this experiment because its transient expression for more than 3 days caused cell death. The fluorescence of PVXΔTGBp1-GFP spread to adjacent cells when MP_{FMV} or SP_{spo}Trun was co-expressed (Fig 5A), indicating that MP_{FMV} and SP_{spo}Trun complemented cell-to-cell movement of PVXΔTGBp1-GFP. Quantitative analysis of fluorescence area suggested significant differences between MP_{FMV} or SP_{spo}Trun and β-glucuronidase (GUS) control (Fig 5B). Categorizing the fluorescence area by the cell number per fluorescent spot also showed significant difference between MP_{FMV} or SP_{spo}Trun and GUS control ($p < 0.01$ by Fisher's exact test). In contrast, the fluorescence of PVXΔTGBp1-GFP was almost confined to a single cell when co-expressed with Trun or SP_{cal}Trun like GUS control (Fig 5A). Comparable expression levels of MP_{FMV} and its mutants were validated by Western blot analysis (Fig 5C). Thus, SP_{spo}Trun, an SP chimera which has the ability to reach PD, complements cell-to-cell movement of PVXΔTGBp1-GFP, indicating that PD localization of MP_{FMV} is necessary to facilitate virus cell-to-cell movement.

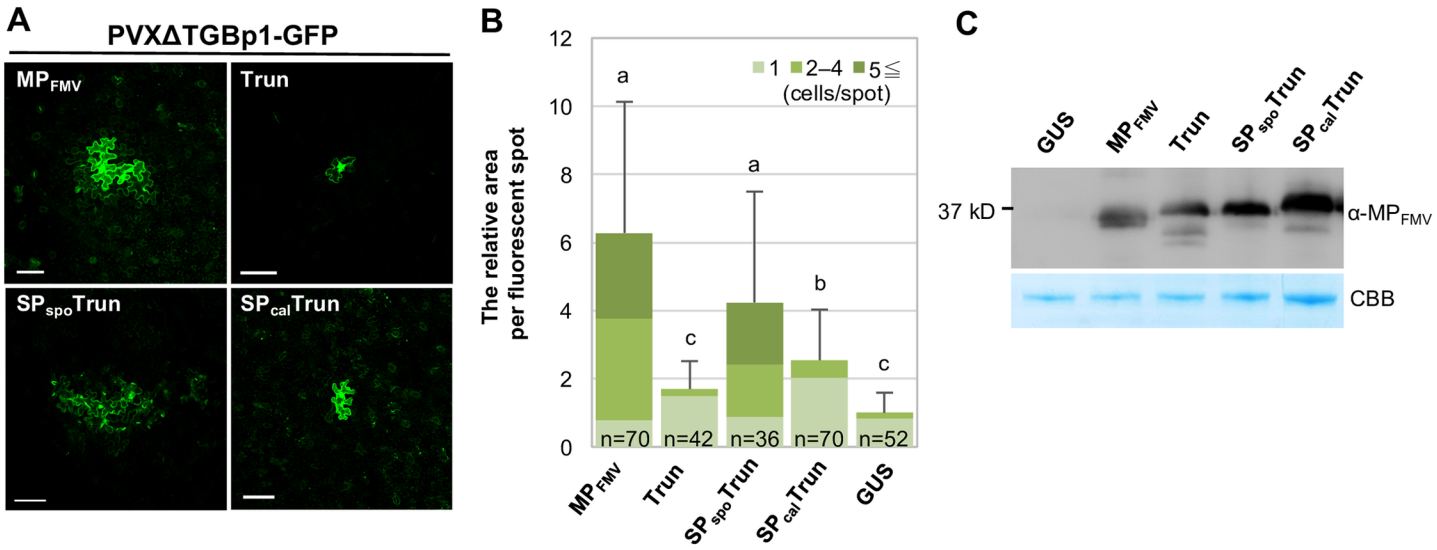

Fig 5. PD localization of MP_{FMV} is necessary to facilitate virus cell-to-cell movement. TGBp1-deficient PVX (PVXΔTGBp1-GFP) was co-expressed with GUS, MP_{FMV} or its mutants (Trun, SP_{spo}Trun or SP_{cal}Trun). (A) Typical images were captured at 5 days post-infiltration (dpi). Bars = 100 μm. (B) Quantification analysis. Measurements were normalized with GUS control; the mean value of GUS-expressing leaves was taken as 1.0. The bars show means + SD. n indicates the total number of measurements in two independent experiments. Different letters on error bars indicate statistical differences at the 1% level of significance (Steel-Dwass test). The fluorescence area is categorized by the cell number per fluorescent spot and shown by different colors. (C) Immunoblot analysis using anti-MP_{FMV} antibody (top panel) confirmed expression of MP_{FMV} and MP_{FMV} mutants. CBB staining is shown as a loading control (bottom panel). Samples were collected at 36 hpi.

https://doi.org/10.1371/journal.ppat.1006463.g005

Most virus MPs are known to move to adjacent cells autonomously [30]. We assessed whether or not these MP_{FMV} mutants were able to move to adjacent cells. MP_{FMV}:YFP and SP_{spo}Trun:YFP spread to adjacent cells when expressed in a single cell (Fig 6A). Conversely,

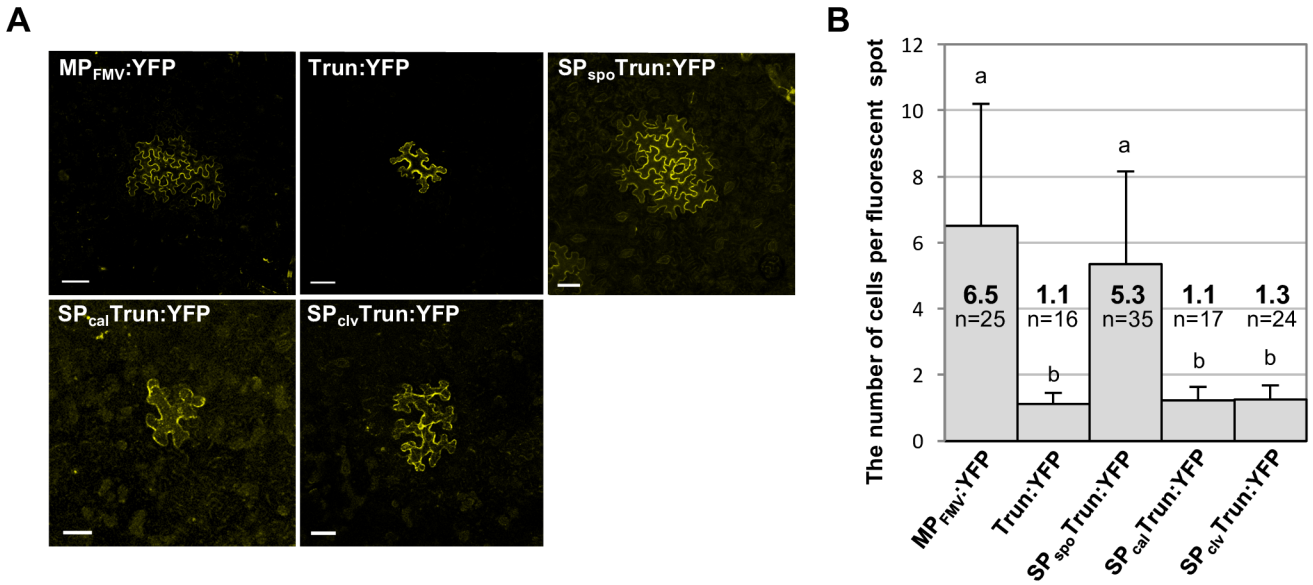

Fig 6. PD localization of MP_{FMV} is necessary for their cell-to-cell movement. Investigation of the ability of MP_{FMV} and its mutants (MP_{FMV}:YFP, Trun:YFP, SP_{spo}Trun:YFP, SP_{cal}Trun:YFP and SP_{clv}Trun:YFP) to move to adjacent cells. (A) Typical images were captured at 3 dpi. Bars = 50 μm. (B) Quantitative analysis. The bars show means + SD. n indicates the total number of measurements in two independent experiments. Different letters on error bars indicate statistical differences at the 1% level of significance (Tukey-Kramer test).

https://doi.org/10.1371/journal.ppat.1006463.g006

Trun:YFP, SP_{cal}Trun:YFP and SP_{clv}Trun:YFP, which do not have the PD-targeting ability, did not move to adjacent cells. Quantitative analysis suggested a significant difference between these two groups in the ability to move to adjacent cells (Fig 6B). These results are in good accordance with virus cell-to-cell complementation assay (Fig 5).

SP-deficient MP_{FMV} localizes to PD when co-expressed with MP_{FMV} or SP chimeras

The experiments described above suggested that the translocation efficiencies determine the subcellular distribution and function of MP_{FMV}. SP_{cal}Trun and SP_{clv}Trun, whose SPs have high translocation efficiencies, localized to the ER, whereas Trun, which does not have an SP, localized to the PM (Table 1). SP_{spo}Trun, which have moderate translocation efficiency, were able to localize to PD in addition to the ER and the PM. Given that SP_{FMV} has low translocation efficiency, a small fraction of MP_{FMV} was probably recruited to the ER. These results allowed us to speculate that co-existence of ER-translocated and non-translocated MP_{FMV} is required for PD localization; in other words, ER-translocated MP_{FMV} and microdomain-localized MP_{FMV} act cooperatively to reach PD.

We tested this hypothesis by co-expressing SP-deficient MP_{FMV} fused with CFP (Trun:CFP) and MP_{FMV}:YFP, Trun:YFP, SP_{spo}Trun:YFP, SP_{cal}Trun:YFP or SP_{clv}Trun:YFP. Localization pattern was not altered when Trun:YFP and Trun:CFP were co-expressed (Fig 7B). By contrast, Trun:CFP was found to localize to punctate structures along the PM when co-expressed with MP_{FMV}:YFP, SP_{spo}Trun:YFP, SP_{cal}Trun:YFP and SP_{clv}Trun:YFP (Fig 7A and 7C–7E). Aniline blue staining confirmed that these punctate structures formed by Trun when co-expressed with MP_{FMV} and SP chimeras coincided with PD (PCC: 0.50 ± 0.06, 0.60 ± 0.06, 0.61 ± 0.05 and 0.56 ± 0.15, respectively; S4 Fig). YFP-fused MP_{FMV} and SP chimeras did not alter their localization by the expression of Trun:CFP. Detailed views showed that SP_{cal}Trun:YFP and SP_{clv}Trun:YFP localized in close proximity to, but did not substantially colocalize with Trun:CFP (Fig 7D and 7E; PCC: 0.31 ± 0.11 and 0.29 ± 0.03, respectively). This localization pattern was similar to those observed when SP_{cal}Trun:YFP or SP_{clv}Trun:YFP was expressed alone (Fig 4Ciii and 4Diii). These results suggest that Trun, which normally localized to the PM, was transported to PD by the function of MP_{FMV} or SP chimeras, which were at least partially translocated to the ER.

The fact that MP_{FMV} or SP chimeras changed Trun localization raised the possibility of the physical interaction between microdomain-localized MP_{FMV} and ER-translocated MP_{FMV}. We have now investigated the interaction between MP_{FMV} and Trun or SP_{clv}Trun using bimolecular fluorescence complementation (BiFC). We first co-expressed the basic leucine zipper transcription factor bZIP63 fused with N-terminal half of YFP (bZIP63:NYF) and with C-terminal half of YFP (bZIP63:CYF) as a control [31]. In this combination, strong fluorescence was observed in the nuclei (S5 Fig). Next, we tested the interaction between MP_{FMV}:NYF and

Table 1. Properties of MP_{FMV} and its mutants.

mutant	translocation efficiency (%)	Localization			cell-to-cell movement (cells)	complementation of virus movement (relative unit)
Trun	no (0)		PM		1.1 ± 0.3	1.7 ± 0.8
MP_{FMV} (wt)	low (4.3 ± 1.5)	(ER)	PM	PD	6.5 ± 3.6	5.6 ± 3.8
SP_{spo}Trun	medium (70.9 ± 0.9)	ER	PM	PD	5.3 ± 2.8	4.2 ± 3.2
SP_{cal}Trun	high (91.9 ± 3.9)	ER			1.1 ± 0.3	2.5 ± 1.4
SP_{clv}Trun	high (93.0 ± 1.6)	ER			1.3 ± 0.4	ND

https://doi.org/10.1371/journal.ppat.1006463.t001

MP_{FMV}:CYF, Trun:CYF or SP_{clv}Trun:CYF. Co-expression of MP_{FMV}:NYF and MP_{FMV}:CYF or Trun:CYF showed a weak fluorescence on the PM. This fluorescence can be ascribed to a background signal or a weak dimerization of microdomain-localized MP_{FMV}. Co-expression of MP_{FMV}:NYF and SP_{clv}Trun:CYF showed no signal, and the physical interaction between microdomain-localized MP_{FMV} and ER-translocated MP_{FMV} was not suggested.

ER-translocated MP_{FMV} specifically localizes to ER-PM contact sites

Given that SP_{cal}Trun:YFP and SP_{clv}Trun:YFP localized in the close proximity to PD (Fig 4Ciii and 4Diii and Fig 7D and 7E), translocated MP_{FMV} appeared to localize in the specific region of the ER. We noticed that the distribution pattern of SP_{cal}Trun:YFP and SP_{clv}Trun:YFP was similar to that of the ER-PM contact site-associated protein, synaptotagmin1 (SYTA) [14,32], which is known to be involved in virus cell-to-cell movement [15–17]. Prior to the co-expression with MP_{FMV}:YFP, we first analyzed localization of SYTA. Co-expression of SYTA:CFP and ER-YFP showed that SYTA:CFP was predominantly distributed to nodes of the ER (PCC = 0.61 ± 0.01; S6A Fig) consistent with the previous reports [14,15]. Aniline blue staining showed that SYTA:CFP was in close proximity to PD (PCC = 0.21 ± 0.01; S6B Fig), which was similar to those seen in SP_{cal}Trun:YFP and SP_{clv}Trun:YFP (Fig 7D and 7E). The close proximity of ER-PM contact sites and PD was reported also in a previous study [32]. To assess whether translocated MP_{FMV} localize to ER-PM contact sites, SYTA:CFP was co-expressed with SP_{clv}Trun:YFP or MP_{FMV}:YFP. SP_{clv}Trun:YFP co-localized almost perfectly with SYTA:CFP, probably in the ER nodes (PCC = 0.54 ± 0.08; Fig 8A). A large fraction of MP_{FMV}:YFP was distributed to the PM and PD, but a small fraction of punctate structures colocalized with SYTA:CFP (Fig 8B). These results show that ER-translocated MP_{FMV} specifically localized to ER-PM contact sites.

To obtain more information about the role of ER-PM contact sites in MP_{FMV} trafficking, we constructed a c-myc tagged $SYTA^{\Delta C2B}$ ($SYTA^{\Delta C2B}$:myc), which is a dominant-negative form lacking the C-terminal 177 aa of SYTA [16]. When MP_{FMV}:YFP was expressed together with $SYTA^{\Delta C2B}$:myc, localization of MP_{FMV}:YFP was apparently affected (Fig 8C and 8D). Although a small fraction of MP_{FMV}:YFP was still retained in PD, a large proportion of MP_{FMV}:YFP excessively accumulated next to PD (PCC = 0.20 ± 0.13; Fig 8C). MP_{FMV}:YFP substantially colocalized with SYTA:CFP in the cortex; instead, fluorescence from MP_{FMV} that localized in the PM microdomains became weaker (PCC = 0.72 ± 0.10; Fig 8D). This result suggests that MP_{FMV}:YFP that normally localized to the PM microdomains aberrantly accumulated in ER-PM contact sites by the expression of $SYTA^{\Delta C2B}$:myc.

We also investigated whether $SYTA^{\Delta C2B}$ affects cell-to-cell movement of MP_{FMV}:YFP. Expression of $SYTA^{\Delta C2B}$:myc inhibited MP_{FMV}:YFP movement to adjacent cells compared with when expressed with GUS (Fig 8Ei and 8Eii). Immunoblot analysis using anti-myc antibody confirmed the expression of $SYTA^{\Delta C2B}$:myc (Fig 8Eiii). Taken together, these data suggest that translocated MP_{FMV} localized to ER-PM contact sites and played an essential role in cell-to-cell movement. To see whether MP_{FMV} interacts with SYTA, BiFC was carried out. Fluorescent signal was not observed when MP_{FMV}:NYF, Trun:NYF and SP_{clv}Trun:NYF were co-expressed with SYTA:CYF (S7 Fig). Thus, the interaction between SYTA and MP_{FMV} or MP_{FMV} mutants was not suggested by BiFC.

MP_{FMV} localization is not affected by inhibiting COPII transport

As the MPs of several viruses use the secretory pathway [9,33], involvement of COPII transport in MP_{FMV} trafficking has been verified by BFA treatment or expression of a dominant-negative form of Sar1 [Sar1(H74L)] [34]. We first confirmed that BFA treatment and Sar1(H74L) expression caused retention of the Golgi marker ManI:CFP [35] in the ER, as expected (S8 Fig). PD

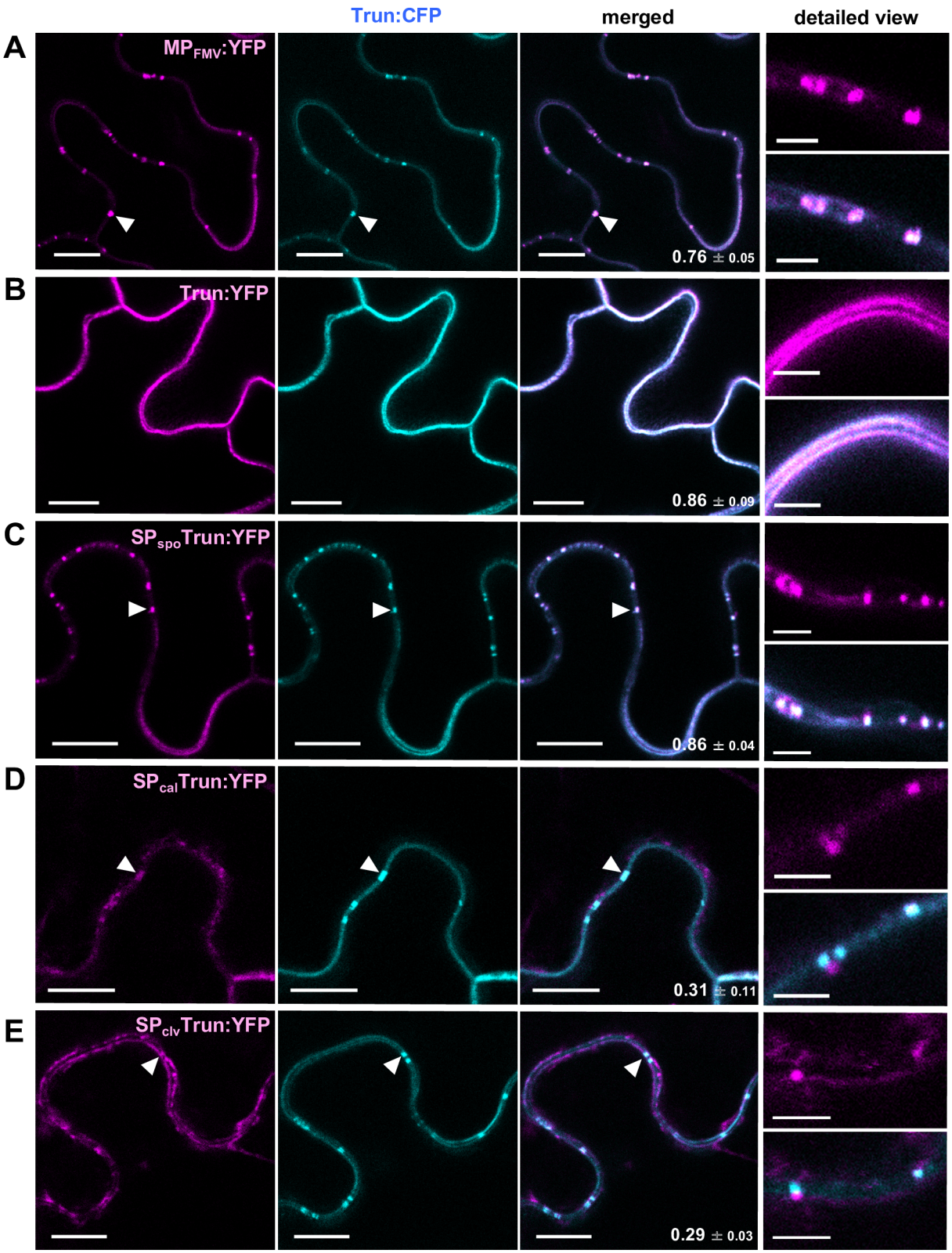

Fig 7. SP-deficient MP$_{FMV}$ localizes to PD when co-expressed with MP$_{FMV}$ or SP chimeras. Trun:CFP was co-expressed with (A) MP$_{FMV}$:YFP, (B) Trun:YFP, (C) SP$_{spo}$Trun:YFP, (D) SP$_{cal}$Trun:YFP or (E) SP$_{clv}$Trun:YFP. Cells were observed at 36 hpi. YFP fluorescence was pseudocolored with magenta. Arrowheads indicate localization to PD. Bars in images of detailed view are 2.5 μm. The others are 10 μm.

https://doi.org/10.1371/journal.ppat.1006463.g007

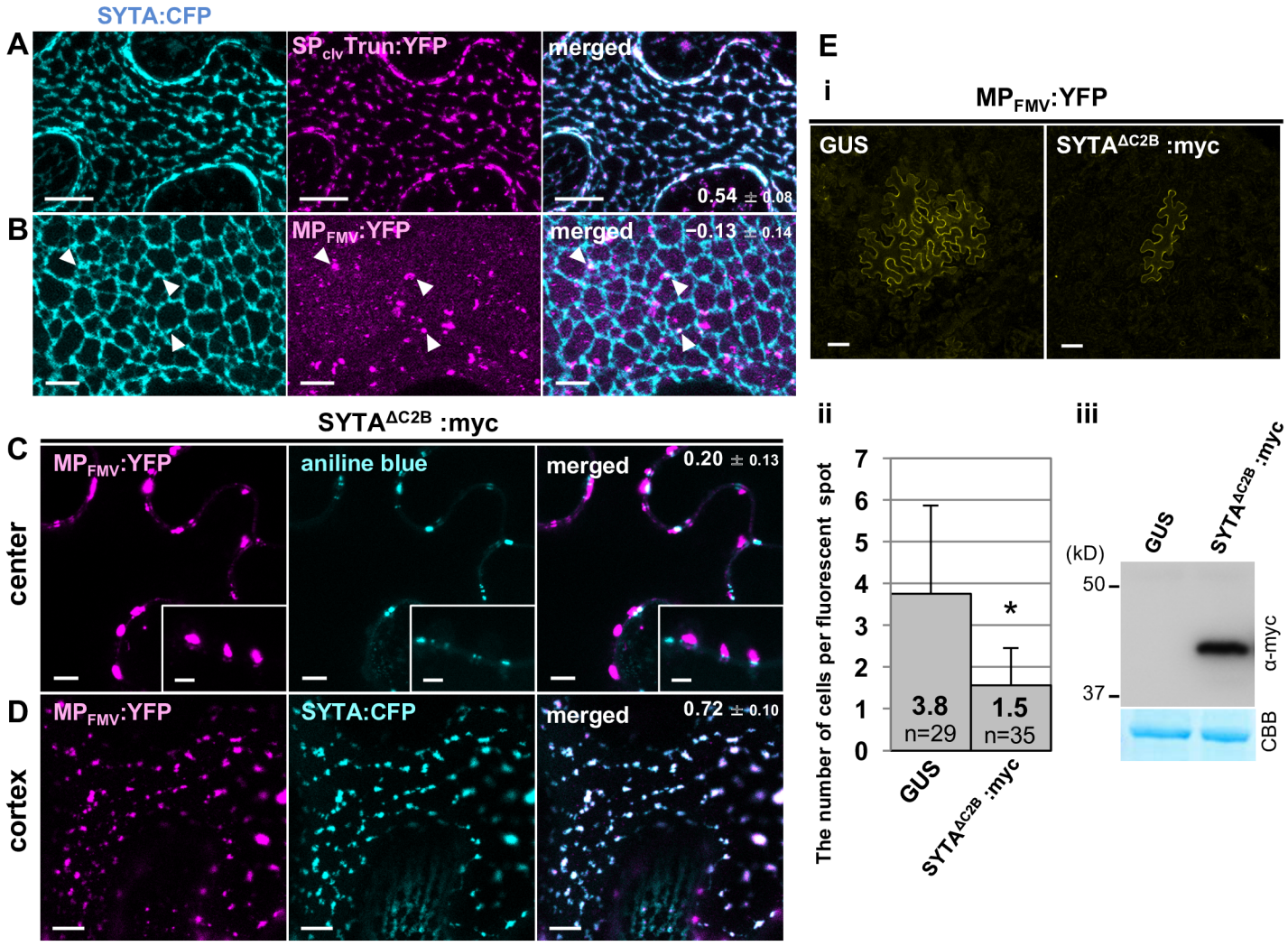

Fig 8. ER-translocated MP_{FMV} specifically localizes to ER-PM contact sites. (A and B) ER-translocated MP_{FMV} co-localized with SYTA, a protein localized to ER-PM contact sites. 3D-projection images of cells expressing SYTA:CFP and (A) SP_{clv}Trun:YFP or (B) MP_{FMV}:YFP. Z-section images of 10 slices at 1.0 μm intervals were processed. Arrowheads indicate co-localization of SYTA:CFP and MP_{FMV}:YFP. (C and D) Expression of $SYTA^{\Delta C2B}$, a dominant-negative form of SYTA, affected MP_{FMV} localization. (C) $SYTA^{\Delta C2B}$:myc was co-expressed with MP_{FMV}:YFP. Plasmodesmata were visualized by aniline blue treatment. (D) $SYTA^{\Delta C2B}$:myc was co-expressed with MP_{FMV}:YFP and SYTA:CFP. A cortical region was visualized. (A–D) Cells were observed at 36 hpi. YFP fluorescence was pseudocolored with magenta. Bars: (A–D), 5 μm; (C) inset 2.5 μm. (E) $SYTA^{\Delta C2B}$:myc showed an inhibitory effect on MP_{FMV} movement to adjacent cells. MP_{FMV}:YFP was co-expressed with GUS or $SYTA^{\Delta C2B}$:myc. (i) Typical images were captured at 3 dpi. Bars = 50 μm. (ii) Quantitative analysis. The bars show means + SD. n indicates the total number of total measurements in two independent experiments. The asterisk above an error bar indicates a statistical difference at the 1% level of significance (Student's t-test). (iii) Immunoblot analysis using anti-myc antibody (top panel). CBB staining is shown as a loading control (bottom panel). Samples were collected at 36 hpi.

https://doi.org/10.1371/journal.ppat.1006463.g008

localization in cells expressing MP_{FMV}:YFP was not affected by BFA treatment or Sar1(H74L) expression. Similarly, inhibiting COPII transport did not affect localization of Trun:YFP in the PM. These results suggest that COPII transport is not involved in the subcellular localization of MP_{FMV} and that MP_{FMV} uses pathways different from BFA-sensitive MPs [9,33].

Discussion

In this study, we analyzed the intracellular trafficking of MP_{FMV}, focusing on SP function, and found that MP_{FMV} targets two subdomains in the ER and PM as well as PD. MP_{FMV}, which

has an N-terminal SP, was distributed mainly in PD and patchy microdomains of the PM (Fig 1 and Fig 2). Investigation of ER translocation efficiency revealed that SP_{FMV} has much lower translocation efficiency compared with those of SP_{spo}, SP_{cal} and SP_{clv} (Fig 3). The SP-deficient mutant (Trun) exclusively localized to the PM microdomains (Fig 4A), whereas two SP chimeras (SP_{cal}Trun and SP_{clv}Trun) exclusively localized to the ER (Fig 4C and 4D). SP_{spo}Trun was distributed in the ER, PM microdomains and PD similar to MP_{FMV}, even though a portion of SP_{spo}Trun aggregated in the ER (Fig 4B). The results so far indicated that MP_{FMV} dually targets the ER and PM due to the inefficient SP; a fraction of MP_{FMV} was successfully translocated into the ER, whereas the remainder of MP_{FMV}, which failed to be translocated, is transferred to the microdomains. This finding led us to speculate that both ER-translocated MP_{FMV} and microdomain-localized MP_{FMV} are necessary for PD localization. Consistent with this notion, the SP-deficient mutant entered into PD by the expression of MP_{FMV} or the SP chimeras, which are able to, at least partially, translocate into the ER (Fig 7). Furthermore, we showed that translocated MP_{FMV} specifically localized to ER-PM contact sites (Fig 8A and 8B), and dominant-negative inhibition of SYTA affected PD localization and cell-to-cell movement of MP_{FMV} (Fig 8C–8E). These results suggest that MP_{FMV} localized to ER-PM contact sites plays an essential role in the entry of microdomain-localized MP_{FMV} into PD. PD localization of MP_{FMV} is necessary to facilitate cell-to-cell movement as shown in the virus movement complementation assay (Fig 5) and the cell-to-cell movement assay (Fig 6). Altogether, we propose a new model for the intracellular trafficking of a viral MP. A substantial proportion of MP_{FMV}, which failed to be translocated, is directly transferred to the microdomains, whereas the remainder of MP_{FMV}, which successfully translocated into the ER, subsequently localizes to ER-PM contact sites and functionally interact with PD to enable microdomain-localized MP_{FMV} to enter into PD (Fig 9).

Dual targeting of MP_{FMV} to the ER and the PM is explained by the low translocation efficiency of the SP_{FMV} (Fig 3). In general, proteins with an SP are co-translationally recognized by the signal recognition particle in the cytosol and recruited to the signal recognition particle receptor on the ER membrane. Then, the Sec61p complex, a channel integrated into the ER membrane, translocates these preproteins into the ER, and subsequently the SP is cleaved by a membrane-bound SP peptidase on the lumenal side [36]. Therefore, the finding that MP_{FMV} was translocated to the ER at a lower rate (approximately 5%; Fig 3) despite the cleavage of SP_{FMV} (Fig 2) is surprising. A substantial proportion of MP_{FMV} molecules probably abort ER translocation after SP cleavage and are released into the cytosol, but further studies are needed to reveal the detailed mechanism of the abortion. In animal cells, it has been reported that an inefficient SP of an ER chaperone calreticulin regulates the ratio of translocated and nontranslocated populations [37]. However, the inefficiency of the animal calreticulin SP is quite moderate, and it generates only a small nontranslocated population. In this regard, to our knowledge, this is the first report of an SP with extremely low efficiency that controls the subcellular distribution of the nascent protein. This low-efficiency SP_{FMV} generates only a small ER-translocated population, but it is probably sufficient for the entry of microdomain-localized MP_{FMV} into PD considering that SP_{spo}Trun:YFP, whose SP has medium translocation efficiency, excessively accumulated in the ER compared with the case of MP_{FMV}:YFP (Fig 4B). SP_{FMV} likely regulates the distribution of MP_{FMV} between the PM and ER in the appropriate proportion.

How is MP_{FMV} associated with two different types of the cellular membrane, the ER membrane and PM? Curiously, a transmembrane domain in MP_{FMV} has not been predicted by SOSUI (http://harrier.nagahama-i-bio.ac.jp/sosui/) and TMHMM server v. 2.0 (http://www.cbs.dtu.dk/services/TMHMM/). Localization of the MP_{FMV} to the PM microdomains is explained as a peripheral membrane protein. Given that the SP-deficient MP_{FMV} was

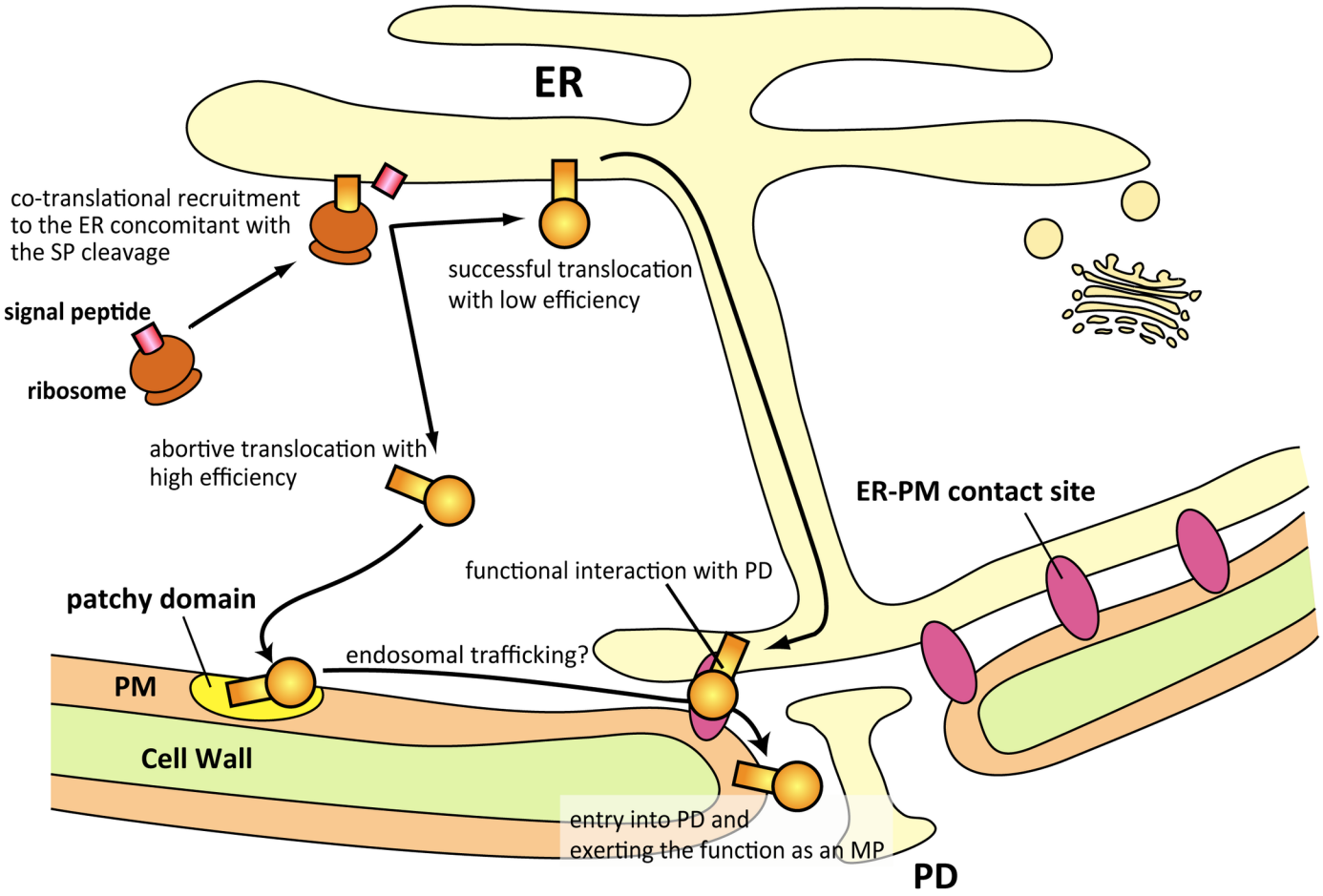

Fig 9. A model for the intracellular trafficking of MP_{FMV}.

https://doi.org/10.1371/journal.ppat.1006463.g009

exclusively associated with the PM microdomains (Fig 4A), even ER translocation is not required to localize to PM microdomains. Microdomain-associated proteins, remorins and flotillins, which do not have SPs and transmembrane domains similarly, are suggested to be peripherally associated with the PM [38–40]. In other words, a transmembrane domain and penetrating the membrane are dispensable for the localization to PM microdomains. The association with the ER membrane is explained by the abnormality of viral proteins. Recent studies on the topology of viral MPs revealed that MPs of tobacco mosaic virus and tomato spotted wilt virus are suggested to be associated with the ER membrane using unusual hydrophobic regions [41–43]. MP_{FMV} may also establish such unconventional hydrophobic regions to be associated with the ER membrane.

Our results raise the question of how two populations of MP_{FMV} that localize to the ER and PM subdomains act cooperatively to gain access to PD. According to BiFC analysis (S7 Fig), physical interaction of these two population is not likely. Although only limited information is available on these membrane subdomains, one possible explanation is that MP_{FMV} in ER-PM contact sites functionally interact with PD, and this might allow the microdomain-localized MP_{FMV} to access into PD (Fig 9). This hypothesis is corroborated by the facts that ER-PM contact sites are spatially close to PD (S6B Fig) [32] and that expression of $SYTA^{\Delta C2B}$, a dominant-negative form of SYTA, affected PD and PM localization of MP_{FMV} (Fig 8C and 8D). In accord

with our results, a previous study showed that, although the localization of 30K was not affected, the cell-to-cell movement of 30K was suppressed in an *Arabidopsis syta* mutant [16]. This study also showed that SYTA$^{\Delta C2B}$ inhibited the formation of endosomes, suggesting that SYTA regulates endocytosis [16]. From these facts, we suspect that MP_{FMV} in the patchy microdomains is transported into PD through endosomal trafficking regulated by SYTA (Fig 9).

The intimate relationship between PD and patchy domains in the PM is implied in this and in other studies. In our study, relocation of the microdomain-localized MP_{FMV} to PD (Fig 7) indicates a functional connection between the patchy microdomains and PD. One previous study about TMV 30K reported that dominant-negative inhibition of class VIII myosins affected PD localization of 30K and induced a patchy distribution in the PM, which did not merge with that of REM1.3 similar to the results from this study [44]. Originally, PM passing through PD is also recognized as a type of microdomain, as it is functionally and spatially distinguished from the surrounding PM [2,45]. Taken together, these two types of PM microdomains, the patchy domains and PM passing through PD, might be functionally connected by ER-PM contact sites.

This study also presents a functional differentiation of MP_{FMV} between the two populations, MP_{FMV} in ER-PM contact sites and PM microdomains. The functional differentiation of a virus MP is reminiscent of the mechanism of cell-to-cell movement regulated by more than one protein. For example, triple gene block movement proteins, which are encoded by viruses belonging to the *Virgaviridae*, *Alphaflexiviridae* and *Betaflexiviridae* families, have specialized functions and perform different tasks for virus cell-to-cell movement: delivering viral factors to PD, interacting with host factors, and increasing PD permeability [46,47]. MP_{FMV} plays multiple roles in cell-to-cell movement using the SP_{FMV} with low translocation efficiency, probably to avoid splitting into modules. This concept may be true also in plant proteins. Although a number of studies have shown that a diverse array of plant proteins have N-terminal SPs, their ER translocation abilities have seldom been investigated. Our findings raise the possibility that SPs can potentially regulate subcellular distribution of the nascent proteins and contribute to protein function in plant cells.

Materials and methods

Transient protein expression

Plasmids expressing GUS, MP_{FMV}, MP_{FMV}:YFP and MP_{FMV}:CFP were prepared as described earlier [23]. Expression vectors of ER-CFP and ER-YFP were purchased from the Arabidopsis Biological Resource Center (Stock numbers CD3-953 and CD3-957, respectively). MP_{FMV} mutant whose SP is not cleaved ($ncMP_{FMV}$) was generated by an PCR using primers containing substitutions to introduce L7P and V11P mutations. $ncMP_{FMV}$ was cloned into pEarleyGate 101 ($ncMP_{FMV}$:YFP) using Gateway technology [48,49]. Trun sequence, which lacks the N-terminal 19 aa of MP_{FMV}, was amplified by PCR and cloned into pEarleyGate 100 (Trun), pEarleyGate 101 (Trun:YFP) and pEarleyGate 102 (Trun:CFP). SP chimera sequences were amplified by PCRs using primers containing each SP sequence, followed by cloning into pEarleyGate 100 (SP_{spo}Trun, SP_{cal}Trun and SP_{clv}Trun) or 101 (SP_{spo}Trun:YFP, SP_{cal}Trun:YFP and SP_{clv}Trun:YFP). In these SP chimeras, the SP region of MP_{FMV} was replaced with the N-terminal sequences of *Ipomoea batatas* sporamin A (M16861; 24 aa) [26], *Nicotiana tabacum* calreticulin (EU984501; 28 aa) [27] or *A. thaliana* CLAVATA3 (AF126009; 22 aa) [28], each of which contains an SP sequence and one aa downstream of the cleavage site. MP_{FMV}:FLAG, in which MP_{FMV} was fused to a FLAG epitope tag immediately downstream of its C terminus, was amplified by PCRs using primers containing FLAG sequence, and cloned into pEarleyGate

100. A 3× N-glycosylation sequon [29] or an ER-retention signal [50] were introduced to the GFP sequence in their C terminus (GFPglc and GFP:HDEL) as was the case with MP_{FMV}:FLAG. The GFP sequence was derived from pEarleyGate 103. The SPs of MP_{FMV}, sporamin A, calreticulin or CLAVATA3 were N-terminally added to GFPglc (SP_{FMV}GFPglc, SP_{spo}GFPglc, SP_{cal}GFPglc and SP_{clv}GFPglc) or GFP:HDEL (SP_{FMV}GFP:HDEL, SP_{spo}GFP:HDEL, SP_{cal}GFP:HDEL and SP_{clv}GFP:HDEL) as was the case with SP chimeras. The REM1.3 (At4g36970) and SYTA (At2g20990) sequences were amplified by PCR from total DNA of *A*. *thaliana*. *REM1.3* was cloned into pEarleyGate 104 (YFP:REM1.3), and *SYTA* was cloned into pEarleyGate 101 (SYTA:YFP) and pEarleyGate 102 (SYTA:CFP). $SYTA^{\Delta C2B}$, a dominant-negative form of *SYTA*, was amplified by PCR according to a previous study [16], and cloned into pEarleyGate Cmyc ($SYTA^{\Delta C2B}$:myc). pEarleyGate Cmyc is an in-house expression vector built from pEarleyGate 101 to introduce a myc tag at the C terminus of a cloned gene. Vectors for BiFC analysis were constructed as shown in the previous study [31]. The TMV MP:GFP sequence (30K:GFP) was amplified from pTMV-MP:GFP [51], and cloned into the pBI121 vector using SalI and BamHI sites.

Plant materials and transient expression

The upper leaves of four-week-old *N*. *benthamiana* plants were used for the transient expression assays. Transient expression was mediated by infiltration of *Agrobacterium tumefaciens* as described previously [23].

Confocal imaging

Cells expressing fluorescent protein fusions were imaged using a Leica TCS SP5 laser-scanning confocal microscope. An HCX PL Apo 63×/1.4–0.6 oil CS lens was used for imaging subcellular localization of fluorescent protein fusions and an HC PL Apo 10×/0.4 CS lens was used for imaging cell-to-cell movement of fluorescent protein fusions. Cells expressing CFP and/or YFP fusions were visualized as described earlier [52]. GFP was excited at the 488-nm argon laser line, and the emission was visualized at 500 to 600 nm. For PM staining, leaves were infiltrated with 50 μM FM4-64 in distilled water, and observed at 1 hpi. FM4-64 was excited at the 543-nm helium/neon laser line, and the emission was visualized at 580 to 650 nm. For PD staining, leaves were infiltrated with 0.1% (w/v) aniline blue in 50 mM sodium phosphate buffer (pH 9.0), and cells were observed at 2 hpi. Aniline blue was excited at the 405-nm laser line, and the emission was visualized at 425 to 480 nm. All the images were acquired at room temperature. Confocal images were processed with LAS AF software version 2.7.3 and Adobe Photoshop CS4. For deconvolution image analysis, between 3 and 8 z-section images at 0.15 μm intervals were captured and processed with Leica Hyvolution system. Fluorescence intensity graphs were generated using the LAS AF quantify intensity tool. PCCs were measured using an Fiji Colocalization plugin [53], and the mean values and standard deviations were calculated from three different images. Generally, PCC values of 0.2–0.4 indicate weak positive correlations and PCC values above 0.5 indicate strong positive correlations [54].

Plasmolysis and inhibition assay

Leaves expressing fluorescent protein fusions were immersed in 4% (w/v) NaCl for 15 min for plasmolysis. For the inhibition assay, leaves were treated with 50 μg/ml BFA in 0.5% (v/v) dimethyl sulfoxide at 18 hpi and observed at 6 h after the treatment.

Quantitative analysis of cell-to-cell movement

A GFP-tagged movement-defective mutant of the PVX infectious clone (PVXΔTGBp1-GFP) [55] was used in the virus movement complementation experiment. Two *Agrobacterium* cultures harboring the binary plasmid expressing GUS, MP_{FMV} or an MP_{FMV} mutant and PVXΔTGBp1-GFP were resuspended and mixed to final concentrations of OD_{600} = 0.4 and 0.0002, respectively. Leaves at 5 dpi were observed under an M165 FC fluorescence stereomicroscope (Leica Microsystems) with an ET GFP filter. Images were captured by a Leica DFC 310 FX camera and LAS software version 4.4.0. The areas of fluorescent foci were measured using ImageJ software version 1.40 (National Institutes of Health). In the assessment of cell-to-cell movement, an *Agrobacterium* culture harboring the binary plasmid expressing MP_{FMV} or its mutants was resuspended and diluted to OD_{600} = 0.0002. When cell-to-cell movement under condition of dominant-negative inhibition of SYTA was investigated, *Agrobacterium* cultures harboring the binary plasmid expressing $SYTA^{\Delta C2B}$:myc or GUS and MP_{FMV}:YFP were resuspended and mixed to final concentrations of OD_{600} = 1.0 and 0.0002, respectively. Leaves at 3 dpi were observed under the laser-scanning confocal microscope as described above.

Detergent treatment of membrane

FMV-infected fig leaves and *N. benthamiana* leaves transiently expressing MP_{FMV}:FLAG or YFP:REM1.3 at 36 hpi were used for isolation of membrane-rich fraction (P30). The fractionation of P30 and chemical treatment were carried out according to the methods of Schaad et al. [56] with minor modifications as follows: Complete Mini (Roche Diagnostics) was added to buffer Q (Lysis Buffer) as a protease inhibitor instead of leupeptin, aprotinin and phenylmethylsulfonyl fluoride. P30 pellets were treated with buffer Q or 1% Triton X-100 (1%[v/v] TritonX-100, 25 mM Tris-HCl [pH 7.5], 150 mM NaCl and 5 mM EDTA).

Immunoprecipitation and immunoblotting

MP_{FMV}:FLAG was immunoprecipitated from cell lysate of *N. benthamiana* leaves expressing MP_{FMV}:FLAG with EZview red anti-FLAG M2 affinity gel (Sigma-Aldrich) [52]. Immunoblot analysis was performed [52] using anti-FLAG M2 antibody (Sigma-Aldrich), anti-myc antibody (EMD Millipore), anti-Bip antibody (Santa Cruz Biotechnology, Inc.), anti-H^+ATPase antibody (Agrisera) or anti-MP_{FMV} antibody. Anti-MP_{FMV} antibody, a polyclonal antibody against the mature region of MP_{FMV}, was generated as described previously [52].

Prediction of signal peptides

SignalP 4.1 software was used to predict SPs [57]. The accession number of MP_{FMV} sequence is BAM13816.

Investigation of ER translocation efficiency

Deglycosylation using endoglycosidase H (Endo H; New England Biolabs) was carried out according to the manufacturer's instructions. Leaves transiently expressing GFPglc, SP_{FMV}GFPglc, SP_{spo}GFPglc, SP_{cal}GFPglc or SP_{clv}GFPglc at 30 hpi were homogenized in 1× glycoprotein denaturing buffer (0.5% SDS and 40 mM DTT), and incubated at 65˚C for 15 min. After removal of cellular debris by centrifugation, the supernatant was suspended in 1× GlycoBuffer 3 (50 mM sodium acetate, pH 6.0) followed by the addition of distilled water or Endo H. After incubation at 37˚C for 1 h, Endo H was inactivated at 75˚C for 10 min. These

samples were analyzed by immunoblotting using anti-GFP antibody (Roche). Signal intensity of each band was quantified using ImageJ software.

Supporting information

S1 Fig. Peptide sequence analysis of the MP_{FMV}:FLAG N terminus. The result of Edman degradation. Letters in the chart indicate peaks corresponding to each amino acid. The N-terminal MP_{FMV} sequence is given below the chart.
(TIF)

S2 Fig. Alignment of SP sequences used in this study. Purple boxes indicate conserved amino acid residues.
(TIF)

S3 Fig. Localization of an MP_{FMV} mutant whose SP is not cleaved. (A) SP prediction of an MP_{FMV} mutant to which L7P and V11P substitutions are introduced ($ncMP_{FMV}$). (B) Localization of $ncMP_{FMV}$:YFP (pseudocolored magenta). (i) A bright-field image was merged. Dotted lines indicate the cell wall (CW). (ii) PD were stained with aniline blue. Cells were observed at 36 hpi. Bars = 5 μm.
(TIF)

S4 Fig. Co-expression of SP-deficient MP_{FMV} and SP chimeras in aniline blue-stained cells. Trun:YFP (pseudocolored magenta) was co-expressed with MP_{FMV}, Trun, SP_{spo}Trun, SP_{cal}-Trun or SP_{clv}Trun. Cells were stained with aniline blue and observed at 36 hpi. Bars = 10 μm.
(TIF)

S5 Fig. Bimolecular fluorescence complementation (BiFC) to investigate the interaction between MP_{FMV} and MP_{FMV} mutants. MP_{FMV}:NYF and MP_{FMV}:CYF, Trun:CYF or SPclvTrun:CYF were co-expressed. bZIP63 was used as a control. Cells were observed at 36 hpi.
(TIF)

S6 Fig. Localization analysis of SYTA. (A) 3D-projection images of cells expressing SYTA:CFP and the ER marker ER-YFP (pseudocolored magenta). Z-section images of 10 slices at 1.0 μm intervals were processed. (B) Aniline blue staining of SYTA:YFP-expressing cells. Cells were observed at 36 hpi. YFP fluorescence was pseudocolored with magenta. Bars: (A), 5 μm; (B) 10 μm; (B) inset 2.5 μm.
(TIF)

S7 Fig. Bimolecular fluorescence complementation (BiFC) to investigate the interaction between MP_{FMV} or MP_{FMV} mutants and SYTA. MP_{FMV}:NYF, Trun:NYF and SPclvTrun:NYF were co-expressed with SYTA:CYF. Cells were observed at 36 hpi. Bars = 25 μm.
(TIF)

S8 Fig. PD localization is not affected by inhibitions of COPII transport. Whether COPII transport is involved in the localization of MP_{FMV}:YFP and Trun:YFP was tested by treatments with 0.5%(v/v) dimethyl sulfoxide (DMSO), 50 μg/ml brefeldin A (BFA) or expression of Sar1(H74L). A Golgi marker, ManI:CFP was used as a control. Cells were observed at 24 hpi. Bars = 10 μm.
(TIF)

Acknowledgments

We thank M. Kuroiwa of the Technology Advancement Center (the Graduate School of Agricultural and Life Sciences, the University of Tokyo) for the Edman sequence analysis. We are

grateful to T. Ueda (the Graduate School of Science, the University of Tokyo) for valuable advice on the analysis of ER translocation efficiency.

Author Contributions

Conceptualization: Kazuya Ishikawa.

Data curation: Kazuya Ishikawa.

Formal analysis: Kazuya Ishikawa.

Funding acquisition: Kazuya Ishikawa, Shigetou Namba.

Investigation: Kazuya Ishikawa, Akira Yusa, Hiroaki Koinuma, Yugo Kitazawa.

Methodology: Kazuya Ishikawa, Osamu Netsu.

Resources: Kazuya Ishikawa.

Supervision: Masayoshi Hashimoto, Osamu Netsu, Yasuyuki Yamaji, Shigetou Namba.

Validation: Kazuya Ishikawa.

Writing – original draft: Kazuya Ishikawa, Masayoshi Hashimoto, Yasuyuki Yamaji, Shigetou Namba.

Writing – review & editing: Kazuya Ishikawa, Yasuyuki Yamaji, Shigetou Namba.

References

1. Maule AJ. Plasmodesmata: structure, function and biogenesis. Curr Opin Plant Biol. 2008; 11: 680–686. https://doi.org/10.1016/j.pbi.2008.08.002 PMID: 18824402
2. Tilsner J, Amari K, Torrance L. Plasmodesmata viewed as specialised membrane adhesion sites. Protoplasma. 2010; 248: 39–60. https://doi.org/10.1007/s00709-010-0217-6 PMID: 20938697
3. Kumar R, Kumar D, Hyun TK, Kim J-Y. Players at plasmodesmal nano-channels. J Plant Biol. 2015; 58: 75–86. https://doi.org/10.1007/s12374-014-0541-z
4. Harries P, Ding B. Cellular factors in plant virus movement: At the leading edge of macromolecular trafficking in plants. Virology. 2011; 411: 237–243. https://doi.org/10.1016/j.virol.2010.12.021 PMID: 21239029
5. Haupt S. Two Plant-Viral Movement Proteins Traffic in the Endocytic Recycling Pathway. Plant Cell. 2005; 17: 164–181. https://doi.org/10.1105/tpc.104.027821 PMID: 15608333
6. Tagami Y, Watanabe Y. Effects of brefeldin A on the localization of Tobamovirus movement protein and cell-to-cell movement of the virus. Virology. 2007; 361: 133–140. https://doi.org/10.1016/j.virol.2006.11.008 PMID: 17174371
7. Kaido M, Tsuno Y, Mise K, Okuno T. Endoplasmic reticulum targeting of the *Red clover necrotic mosaic virus* movement protein is associated with the replication of viral RNA1 but not that of RNA2. Virology. 2009; 395: 232–242. https://doi.org/10.1016/j.virol.2009.09.022 PMID: 19819513
8. Harries PA, Schoelz JE, Nelson RS. Intracellular transport of viruses and their components: utilizing the cytoskeleton and membrane highways. Mol Plant Microbe In. 2010; 23: 1381–1393. https://doi.org/10.1094/MPMI-05-10-0121 PMID: 20653412
9. Genovés A, Navarro JA. The intra-and intercellular movement of *Melon necrotic spot virus* (MNSV) depends on an active secretory pathway. Mol Plant Microbe In. 2010; 23: 263–272. https://doi.org/10.1094/MPMI-23-3-0263 PMID: 20121448
10. Huang Z, Han Y, Howell SH. Formation of Surface Tubules and Fluorescent Foci in *Arabidopsis thaliana* Protoplasts Expressing a Fusion between the Green Fluorescent Protein and the Cauliflower Mosaic Virus Movement Protein. Virology. 2000; 271: 58–64. https://doi.org/10.1006/viro.2000.0292 PMID: 10814570
11. Pouwels J, Van Der Krogt GNM, Van Lent J, Bisseling T, Wellink J. The Cytoskeleton and the Secretory Pathway Are Not Involved in Targeting the Cowpea Mosaic Virus Movement Protein to the Cell Periphery. Virology. 2002; 297: 48–56. https://doi.org/10.1006/viro.2002.1424 PMID: 12083835

12. Carluccio AV, Zicca S, Stavolone L. Hitching a Ride on Vesicles: Cauliflower Mosaic Virus Movement Protein Trafficking in the Endomembrane System. Plant Physiol. 2014; 164: 1261–1270. https://doi.org/10.1104/pp.113.234534 PMID: 24477592

13. Prinz WA. Bridging the gap: membrane contact sites in signaling, metabolism, and organelle dynamics. J Cell Biol. 2014; 205: 759–769. https://doi.org/10.1083/jcb.201401126 PMID: 24958771

14. Pérez-Sancho J, Vanneste S, Lee E, McFarlane HE, Esteban del Valle A, Valpuesta V, et al. The Arabidopsis Synaptotagmin1 Is Enriched in Endoplasmic Reticulum-Plasma Membrane Contact Sites and Confers Cellular Resistance to Mechanical Stresses. Plant Physiol. 2015; 168: 132–143. https://doi.org/10.1104/pp.15.00260 PMID: 25792253

15. Levy A, Zheng JY, Lazarowitz SG. Synaptotagmin SYTA Forms ER-Plasma Membrane Junctions that Are Recruited to Plasmodesmata for Plant Virus Movement. Curr Biol. 2015; 25: 2018–2025. https://doi.org/10.1016/j.cub.2015.06.015 PMID: 26166780

16. Lewis JD, Lazarowitz SG. *Arabidopsis* synaptotagmin SYTA regulates endocytosis and virus movement protein cell-to-cell transport. Proc Natl Acad Sci U S A. 2010; 107: 2491–2496. https://doi.org/10.1073/pnas.0909080107 PMID: 20133785

17. Uchiyama A, Shimada-Beltran H, Levy A, Zheng JY, Javia PA, Lazarowitz SG. The Arabidopsis synaptotagmin SYTA regulates the cell-to-cell movement of diverse plant viruses. Front Plant Sci. 2014; 5: 584. https://doi.org/10.3389/fpls.2014.00584 PMID: 25414709

18. Malinsky J, Opekarová M, Grossmann G, Tanner W. Membrane Microdomains, Rafts, and Detergent-Resistant Membranes in Plants and Fungi. Annu Rev Plant Biol. 2013; 64: 501–529. https://doi.org/10.1146/annurev-arplant-050312-120103 PMID: 23638827

19. Jarsch IK, Konrad SSA, Stratil TF, Urbanus SL, Szymanski W, Braun P, et al. Plasma Membranes Are Subcompartmentalized into a Plethora of Coexisting and Diverse Microdomains in *Arabidopsis* and *Nicotiana benthamiana*. Plant Cell. 2014; 26: 1698–1711. https://doi.org/10.1105/tpc.114.124446 PMID: 24714763

20. Raffaele S, Bayer E, Lafarge D, Cluzet S, German Retana S, Boubekeur T, et al. Remorin, a Solanaceae Protein Resident in Membrane Rafts and Plasmodesmata, Impairs Potato virus X Movement. Plant Cell. 2009; 21: 1541–1555. https://doi.org/10.1105/tpc.108.064279 PMID: 19470590

21. Heijne von G. The signal peptide. J Membrane Biol. 1990; 115: 195–201. https://doi.org/10.1007/BF01868635

22. Kim DH, Hwang I. Direct Targeting of Proteins from the Cytosol to Organelles: The ER versus Endosymbiotic Organelles. Traffic. 2013; 14: 613–621. https://doi.org/10.1111/tra.12043 PMID: 23331847

23. Ishikawa K, Maejima K, Komatsu K, Netsu O, Keima T, Shiraishi T, et al. Fig mosaic emaravirus p4 protein is involved in cell-to-cell movement. J Gen Virol. 2013; 94: 682–686. https://doi.org/10.1099/vir.0.047860-0 PMID: 23152372

24. Oparka KJ, Prior DAM, Crawford JW. Behaviour of plasma membrane, cortical ER and plasmodesmata during plasmolysis of onion epidermal cells. Plant Cell Environ. 1994; 17: 163–171. https://doi.org/10.1111/j.1365-3040.1994.tb00279.x

25. Mongrand S, Morel J, Laroche J, Claverol S, Carde JP, Hartmann MA, et al. Lipid Rafts in Higher Plant Cells: Purification and characterization of Triton X-100-insoluble microdomains from tobacco plasma membrane. J Biol Chem. 2004; 279: 36277–36286. https://doi.org/10.1074/jbc.M403440200 PMID: 15190066

26. Hattori T, Nakagawa T, Maeshima M, Nakamura K, Asahi T. Molecular cloning and nucleotide sequence of cDNA for sporamin, the major soluble protein of sweet potato tuberous roots. Plant Mol Biol. 1985; 5: 313–320. https://doi.org/10.1007/BF00020629 PMID: 24306923

27. Henderson RA, Michel H, Sakaguchi K, Shabanowitz J, Appella E, Hunt DF, et al. HLA-A2.1-associated peptides from a mutant cell line: a second pathway of antigen presentation. Science. 1992; 255: 1264–1266. PMID: 1546329

28. Fletcher JC, Brand U, Running MP, Simon R, Meyerowitz EM. Signaling of cell fate decisions by *CLAVATA3* in *Arabidopsis* shoot meristems. Science. 1999; 283: 1911–1914. PMID: 10082464

29. Bañó-Polo M, Baldin F, Tamborero S, Marti-Renom MA, Mingarro I. N-glycosylation efficiency is determined by the distance to the C-terminus and the amino acid preceding an Asn-Ser-Thr sequon. Protein Sci. 2010; 20: 179–186. https://doi.org/10.1002/pro.551 PMID: 21082725

30. Lazarowitz SG, Beachy RN. Viral Movement Proteins as Probes for Intracellular and Intercellular Trafficking in Plants. Plant Cell. 1999; 11: 535. https://doi.org/10.2307/3870882 PMID: 10213776

31. Maejima K, Iwai R, Himeno M, Komatsu K, Kitazawa Y, Fujita N, et al. Recognition of floral homeotic MADS domain transcription factors by a phytoplasmal effector, phyllogen, induces phyllody. Plant J. 2014; 78: 541–554. https://doi.org/10.1111/tpj.12495 PMID: 24597566

32. Schapire AL, Voigt B, Jasik J, Rosado A, Lopez-Cobollo R, Menzel D, et al. *Arabidopsis* synaptotagmin 1 is required for the maintenance of plasma membrane integrity and cell viability. Plant Cell. 2008; 20: 3374–3388. https://doi.org/10.1105/tpc.108.063859 PMID: 19088329

33. Laporte C. Involvement of the Secretory Pathway and the Cytoskeleton in Intracellular Targeting and Tubule Assembly of *Grapevine fanleaf virus* Movement Protein in Tobacco BY-2 Cells. Plant Cell. 2003; 15: 2058–2075. https://doi.org/10.1105/tpc.013896 PMID: 12953111

34. Takeuchi M, Tada M, Saito C, Yashiroda H, Nakano A. Isolation of a Tobacco cDNA Encoding Sar1 GTPase and Analysis of Its Dominant Mutations in Vesicular Traffic Using a Yeast Complementation System. Plant Cell Physiol. 1998; 39: 590–599. PMID: 9697342

35. Nelson BK, Cai X, Nebenführ A. A multicolored set of *in vivo* organelle markers for co-localization studies in Arabidopsis and other plants. Plant J. 2007; 51: 1126–1136. https://doi.org/10.1111/j.1365-313X.2007.03212.x PMID: 17666025

36. Hegde RS, Bernstein HD. The surprising complexity of signal sequences. Trends Biochem Sci. 2006; 31: 563–571. https://doi.org/10.1016/j.tibs.2006.08.004 PMID: 16919958

37. Shaffer KL, Sharma A, Snapp EL, Hegde RS. Regulation of Protein Compartmentalization Expands the Diversity of Protein Function. Dev Cell. 2005; 9: 545–554. https://doi.org/10.1016/j.devcel.2005.09.001 PMID: 16198296

38. Jarsch IK, Ott T. Perspectives on remorin proteins, membrane rafts, and their role during plant-microbe interactions. Mol Plant Microbe In. 2011; 24: 7–12. https://doi.org/10.1094/MPMI-07-10-0166 PMID: 21138374

39. Li R, Liu P, Wan Y, Chen T, Wang Q, Mettbach U, et al. A Membrane Microdomain-Associated Protein, *Arabidopsis* Flot1, Is Involved in a Clathrin-Independent Endocytic Pathway and Is Required for Seedling Development. Plant Cell. 2012; 24: 2105–2122. https://doi.org/10.1105/tpc.112.095695 PMID: 22589463

40. Kurrle N, John B, Meister M, Tikkanen R. Function of flotillins in receptor tyrosine kinase signaling and endocytosis: role of tyrosine phosphorylation and oligomerization. Rijeka: INTECH Open Access Publisher, 2012. 307–342.

41. Peiro A, Martinez-Gil L, Tamborero S, Pallás V, Sanchez-Navarro JA, Mingarro I, et al. The *Tobacco mosaic virus* Movement Protein Associates with but Does Not Integrate into Biological Membranes. J Virol. 2014; 88: 3016–3026. https://doi.org/10.1128/JVI.03648-13 PMID: 24371064

42. Leastro MO, Pallás V, Resende RO, Sanchez-Navarro JA. The movement proteins (NSm) of distinct tospoviruses peripherally associate with cellular membranes and interact with homologous and heterologous NSm and nucleocapsid proteins. Virology. 2015; 478: 39–49. https://doi.org/10.1016/j.virol.2015.01.031 PMID: 25705793

43. Feng Z, Xue F, Xu M, Chen X, Zhao W, Garcia-Murria MJ, et al. The ER-Membrane Transport System Is Critical for Intercellular Trafficking of the NSm Movement Protein and Tomato Spotted Wilt Tospovirus. PLoS Pathog. 2016; 12: e1005443. https://doi.org/10.1371/journal.ppat.1005443 PMID: 26863622

44. Amari K, Di Donato M, Dolja VV, Heinlein M. Myosins VIII and XI Play Distinct Roles in Reproduction and Transport of *Tobacco Mosaic Virus*. PLoS Pathog. 2014; 10: e1004448–15. https://doi.org/10.1371/journal.ppat.1004448 PMID: 25329993

45. Grison MS, Brocard L, Fouillen L, Nicolas W, Wewer V, Dörmann P, et al. Specific membrane lipid composition is important for plasmodesmata function in Arabidopsis. Plant Cell. 2015; 27: 1228–1250. https://doi.org/10.1105/tpc.114.135731 PMID: 25818623

46. Verchot-Lubicz J, Torrance L, Solovyev AG, Morozov SY, Jackson AO, Gilmer D. Varied movement strategies employed by triple gene block-encoding viruses. Mol Plant Microbe In. 2010; 23: 1231–1247. https://doi.org/10.1094/MPMI-04-10-0086 PMID: 20831404

47. Park M-R, Jeong R-D, Kim K-H. Understanding the intracellular trafficking and intercellular transport of potexviruses in their host plants. Front Plant Sci. 2014; 5: 60. https://doi.org/10.3389/fpls.2014.00060 PMID: 24672528

48. Earley KW, Haag JR, Pontes O, Opper K, Juehne T, Song K, et al. Gateway-compatible vectors for plant functional genomics and proteomics. Plant J. 2006; 45: 616–629. https://doi.org/10.1111/j.1365-313X.2005.02617.x PMID: 16441352

49. Hashimoto M, Komatsu K, Maejima K, Okano Y, Shiraishi T, Ishikawa K, et al. Identification of three MAPKKKs forming a linear signaling pathway leading to programmed cell death in *Nicotiana benthamiana*. BMC Plant Biol. 2012; 12: 1. https://doi.org/10.1186/1471-2229-12-1

50. The C-terminal HDEL sequence is sufficient for retention of secretory proteins in the endoplasmic reticulum (ER) but promotes vacuolar targeting of proteins that escape the ER. Plant J. 1997; 11: 313–325. PMID: 9076996

51. Yoshii A, Shimizu T, Yoshida A, Hamada K, Sakurai K, Yamaji Y, et al. NTH201, a novel class II KNOTTED1-like protein, facilitates the cell-to-cell movement of *Tobacco mosaic virus* in tobacco. Mol Plant Microbe In. 2008; 21: 586–596. https://doi.org/10.1094/MPMI-21-5-0586 PMID: 18393618

52. Ishikawa K, Miura C, Maejima K, Komatsu K, Hashimoto M, Tomomitsu T, et al. Nucleocapsid protein from fig mosaic virus forms cytoplasmic agglomerates that are hauled by endoplasmic reticulum streaming. J Gen Virol 2015; 89: 480–491. https://doi.org/10.1128/JVI.02527-14 PMID: 25320328

53. Schindelin J, Arganda-Carreras I, Frise E, Kaynig V, Longair M, Pietzsch T, et al. Fiji: an open-source platform for biological-image analysis. Nat Meth. 2012; 9: 676–682. https://doi.org/10.1038/nmeth.2019 PMID: 22743772

54. Anonymous. Resources for online and print readers. Chapter 11. Correlation and regression. BMJ. 2017. Available from: http://www.bmj.com/about-bmj/resources-readers/publications/statistics-square-one/11-correlation-and-regression.

55. Senshu H, Yamaji Y, Minato N, Shiraishi T, Maejima K, Hashimoto M, et al. A Dual Strategy for the Suppression of Host Antiviral Silencing: Two Distinct Suppressors for Viral Replication and Viral Movement Encoded by Potato Virus M. J Virol. 2011; 85: 10269–10278. https://doi.org/10.1128/JVI.05273-11 PMID: 21752911

56. Schaad MC, Jensen PE, Carrington JC. Formation of plant RNA virus replication complexes on membranes: role of an endoplasmic reticulum-targeted viral protein. EMBO J. 1997; 16: 4049–4059. https://doi.org/10.1093/emboj/16.13.4049 PMID: 9233814

57. Petersen TN, Brunak S, Heijne von G, Nielsen H. SignalP 4.0: discriminating signal peptides from transmembrane regions. Nat Meth. 2011; 8: 785–786. https://doi.org/10.1038/nmeth.1701 PMID: 21959131